Cardiovascular Interventions in Clinical Practice

EDITED BY

Jürgen Haase MD, PhD, FESC, FACC
Professor of Medicine, Consultant Cardiologist
Kardiocentrum Frankfurt
Klinik Rotes Kreuz
Frankfurt/Main, Germany

Hans-Joachim Schäfers MD, PhD
Professor of Surgery
Chair, Department of Thoracic and Cardiovascular Surgery
University Hospital Saarland
Homburg/Saar, Germany

Horst Sievert MD, FESC, FACC
Professor of Medicine
Head, Department of Cardiology
CardioVascular Center Frankfurt
Frankfurt, Germany

Ron Waksman MD, FACC
Professor of Medicine
Associate Director, Division of Cardiology
Director, Experimental Cardiology
Washington Hospital Center
Washington, DC, USA

WILEY-BLACKWELL
A John Wiley & Sons, Ltd., Publication

Cardiovascular Interventions in Clinical Practice

Cardiovascular Interventions in Clinical Practice

EDITED BY

Jürgen Haase MD, PhD, FESC, FACC
Professor of Medicine, Consultant Cardiologist
Kardiocentrum Frankfurt
Klinik Rotes Kreuz
Frankfurt/Main, Germany

Hans-Joachim Schäfers MD, PhD
Professor of Surgery
Chair, Department of Thoracic and Cardiovascular Surgery
University Hospital Saarland
Homburg/Saar, Germany

Horst Sievert MD, FESC, FACC
Professor of Medicine
Head, Department of Cardiology
CardioVascular Center Frankfurt
Frankfurt, Germany

Ron Waksman MD, FACC
Professor of Medicine
Associate Director, Division of Cardiology
Director, Experimental Cardiology
Washington Hospital Center
Washington, DC, USA

WILEY-BLACKWELL
A John Wiley & Sons, Ltd., Publication

This edition first published 2010 © by Blackwell Publishing Ltd

Blackwell Publishing was acquired by John Wiley & Sons in February 2007. Blackwell's publishing program has been merged with Wiley's global Scientific, Technical and Medical business to form Wiley-Blackwell.

Registered office: John Wiley & Sons Ltd, The Atrium, Southern Gate, Chichester, West Sussex, PO19 8SQ, UK

Editorial offices: 9600 Garsington Road, Oxford, OX4 2DQ, UK
The Atrium, Southern Gate, Chichester, West Sussex, PO19 8SQ, UK
111 River Street, Hoboken, NJ 07030-5774, USA

For details of our global editorial offices, for customer services and for information about how to apply for permission to reuse the copyright material in this book please see our website at www.wiley.com/wiley-blackwell

Library of Congress Cataloging-in-Publication Data
Cardiovascular interventions in clinical practice / edited by Jürgen Haase. — 1st ed.
p. ; cm.
Includes bibliographical references and index.
ISBN 978-1-4051-8277-5 (hardcover : alk. paper)
1. Cardiovascular system—Diseases—Treatment. 2. Heart—Surgery. I. Haase, Jürgen, Prof. Dr.
[DNLM: 1. Cardiovascular Diseases—therapy. 2. Cardiac Surgical Procedures. 3. Cardiovascular Diseases—diagnosis. 4. Cardiovascular Diseases—pathology. WG 166 C2663 2009]
RC669.C2863 2009
616.1'06—dc22

2009032166

ISBN: 9781405182775

A catalogue record for this book is available from the British Library.
Set in 9/12pt Meridien by Graphicraft Limited, Hong Kong
Printed and bound in Singapore

1 2010

Contents

List of Contributors

Suhny Abbara MD
Assistant Professor, Harvard Medical School
Director of Cardiovascular Imaging Section, Massachusetts General Hospital
Director of Education, Cardiac MR/PET/CT Program
Boston, MA, USA

Pierfrancesco Agostoni MD
Department of Cardiology
University Medical Center Utrecht
Utrecht, The Netherlands

Diana Aicher MD
Department of Thoracic and Cardiovascular Surgery
University Hospital of Saarland
Homburg/Saar, Germany

Ibrahim Akin MD
Department of Medicine
Division of Cardiology at the University Hospital Rostock
Rostock School of Medicine
Rostock, Germany

Seth Assar MD
St. Luke's Medical Center
Phoenix, AZ
University of Arizona
Tucson, AZ, USA

Birgit Assmus MD
Division of Cardiology
University Hospital Frankfurt/Main
Frankfurt/Main, Germany

Anirban Banerjee MD
Center for Cardiovascular Imaging
Tufts University Medical Center
Boston, MA, USA

Peter Barlis MD
Department of Cardiology
Royal Brompton Hospital
London, UK

Thomas Bartel MD
Cardiology Division
Department of Internal Medicine III
Medical University of Innsbruck
Innsbruck
Austria

Philipp Beerbaum MD
Senior Clinical Lecturer
King's College London
Consultant Paediatric Cardiologist
The Evelina Children's Hospital
London, UK

Robert H. Boone MD
Interventional Cardiology
St. Paul's Hospital
University of British Columbia
Vancouver, Canada

Marc Bosiers MD
Department of Vascular Surgery
AZ St-Blasius
Dendermonde, Belgium

Jagdish Butany MD
McLaughlin Centre for Molecular Medicine
University of Toronto
Department of Pathology
University Health Network
Toronto, Ontario, Canada

Sara D. Collins MD
Washington Hospital Center
Division of Cardiology
Washington, DC, USA

Stefano De Castro MD
Center for Cardiovascular Imaging
Tufts University Medical Center
Boston, MA, USA

Koen Deloose MD
Department of Vascular Surgery
AZ St-Blasius
Dendermonde, Belgium

Carlo Di Mario MD, PhD
Professor of Medicine
Consultant Cardiologist
Royal Brompton Hospital
London, UK

Mirko Doss MD
J.W. Goethe University
Frankfurt/Main, Germany

Maria Drakopoulou MD
Department of Cardiology
Hippokration Hospital
Athens Medical School
Athens, Greece

Savio D'Souza MD
Department of Cardiology
Royal Brompton Hospital
London, UK

Anthony L. Estrera MD
Department of Cardiothoracic and Vascular Surgery
University of Texas at Houston Medical School
Memorial Hermann Heart and Vascular Institute
Houston, TX, USA

Antonietta Evangelista MD
Center for Cardiovascular Imaging
Tufts University Medical Center
Boston, MA, USA

Francesco F. Faletra MD
Center for Cardiovascular Imaging
Tufts University Medical Center
Boston, MA, USA

Paul Fefer MD
The Schulich Heart Programme
Sunnybrook Research Institute
Sunnybrook Health Sciences Centre
Toronto, Ontario, Canada

Wolfgang Fehske MD
Associate Professor of Medicine
Head, Department of Cardiology
St. Vinzenz-Hospital
Cologne, Germany

Ted Feldman MD, FACC, FSCAI
Professor of Medicine
Chair, Interventional Cardiology
Evanston Northwestern Health Care
Cardiovascular Institute
Mt View, CA, USA

Giuseppe Ferrante MD
Department of Cardiology
Royal Brompton Hospital
London, UK

Michael C. Fishbein MD
Piansky Professor of Pathology and Medicine
Department of Pathology and Laboratory Medicine
David Geffen School of Medicine at UCLA
Los Angeles, CA, USA

Jennifer Franke MD
CardioVascular Center Frankfurt
Frankfurt, Germany

Hector M. Garcia-Garcia MD, MSc
Thoraxcenter
Erasmus Medical Center
Rotterdam, The Netherlands

Nikolaus Gassler MD, MA
Professor of Pathology
Institute of Pathology
RWTH Aachen University
Aachen, Germany

Anne L. Gaster MD, PhD
Thoraxcenter
Erasmus Medical Center
Rotterdam, The Netherlands

Ramil Goel MD
Banner Good Samaritan Medical Center
Phoenix, AZ, USA

Nieves Gonzalo MD
Thoraxcenter
Erasmus Medical Center
Rotterdam, The Netherlands

Kevin L. Greason MD
Department of Cardiovascular Surgery
Mayo Clinic
Rochester, MN, USA

Matthias Gutberlet MD, PhD
Professor of Radiology
Director of the Department of Diagnostic and Interventional Radiology
University Leipzig/Leipzig Heart Center
Leipzig, Germany

Juan Luis Gutiérrez-Chico MD, PhD, FESC
Interventional Cardiology Unit
Vigo University Hospital
Vigo, Spain

Jürgen Haase MD, PhD, FESC, FACC
Professor of Medicine, Consultant Cardiologist
Kardiocentrum Frankfurt
Klinik Rotes Kreuz
Frankfurt/Main, Germany

Markus K. Heinemann MD, PhD
Professor of Pediatric Cardiac Surgery
University Hospital
Johannes Gutenberg University Mainz
Mainz, Germany

Esther Herpel MD
Institute of Pathology
University Clinics Heidelberg
Germany

Richard R. Heuser MD, FACC, FACP, FESC, FASCI
Director of Cardiology St. Luke's Hospital and Medical Center
Clinical Professor of Medicine, University of Arizona College of Medicine
Phoenix, AZ, USA

Siew Yen Ho PHD, FRCPath, FESC
Professor and Head of Cardiac Morphology Unit
Royal Brompton Hospital and Imperial College London
London, UK

L. Nelson Hopkins MD
Professor and Chairman of Neurosurgery and Professor of Radiology
Department of Neurosurgery and Radiology and Toshiba Stroke Research Center
School of Medicine and Biomedical Sciences
University of Buffalo, State University of New York
Department of Neurosurgery, Millard Fillmore Gales Hospital, Kaleida Health
Buffalo, NY, USA

Christian Ihling MD
Professor of Medicine
Gemeinschaftspraxis für Pathologie
Frankfurt/Main
Germany

Hüseyin Ince MD
Department of Medicine
Division of Cardiology at the University Hospital Rostock
Rostock School of Medicine
Rostock, Germany

Ignacio Inglessis MD
Adult Congenital Heart Disease Program
Department of Cardiology
Massachusetts General Hospital
Boston, MA, USA

Pascal Jabbour MD
Department of Neurosurgery
Thomas Jefferson University Hospital
Jefferson Hospital for Neuroscience
Philadelphia, PA, USA

Saibal Kar MD, FACC, FSCAI
Evanston Northwestern Health Care
Cardiovascular Institute
Mt View, CA, USA

Osamu Katoh MD
Director of Research Center
Toyohashi Heart Center
Toyohashi, Aichi, Japan

Martin G. Keane MD
Cardiovascular Division
Department of Medicine
University of Pennsylvania School of Medicine
Philadelphia, PA, USA

Prafulla G. Kerkar MD
Professor and Head
Department of Cardiology
Seth GS Medical College and KEM Hospital
Mumbai, India

Kourosh Keyhani MD
Department of Cardiothoracic and Vascular Surgery
The University of Texas at Houston Medical School
Memorial Hermann Heart and Vascular Institute
Houston, TX, USA

Carey Kimmelstiel MD
Center for Cardiovascular Imaging
Tufts University Medical Center
Boston, MA, USA

Stephan Kische MD
Department of Medicine
Division of Cardiology at the University Hospital Rostock
Rostock School of Medicine
Rostock, Germany

Michael J. Kostal MD
Cardiovascular Division
Department of Medicine
University of Pennsylvania School of Medicine
PA, USA

Neville Kukreja MA, MRCP
Thoraxcenter
Erasmus Medical Center
Rotterdam, The Netherlands

Takashi Kunihara MD, PhD
Department of Thoracic and Cardiovascular Surgery
University Hospital of Saarland
Homburg, Germany

Chi K. Lai MD, FRCPC
Assistant Professor of Pathology
Department of Pathology and Laboratory Medicine
David Geffen School of Medicine at UCLA
Los Angeles, CA, USA

Katharina Lehn
Cardiovascular Center Frankfurt
Frankfurt, Germany

Elad I. Levy MD
Associate Professor of Neurosurgery and Radiology
Departments of Neurosurgery and Radiology and Toshiba Stroke Research Center
University at Buffalo, State University of New York
Department of Neurosurgery
Millard Fillmore Gates Hospital, Kaleida Health
Buffalo, NY, USA

Faqian Li MD, PhD
Assistant Professor
Department of Pathology and Laboratory Medicine
University of Rochester Medical Center,
Rochester, NY, USA

Artur Lichtenberg MD, PhD
Clinic for Cardiovascular Surgery
University of Düsseldorf
Düsseldorf, Germany

Christos Lioupis MD
Department of Vascular Surgery
AZ St-Blasius
Dendermonde, Belgium

Joachim Lotz MD
Institute of Radiology
Hannover Medical School
Hannover, Germany

Suntharo Ly MD
St. Luke's Medical Center
Phoenix, AZ
University of Arizona
Tucson, AZ, USA

Shawn McMahon PA, MPH
Center for Vascular Care
Washington Hospital Center
Washington, DC, USA

Pedro Marcos-Alberca MD, PhD
Cardiovascular Imaging Unit
Hospital Clinico San Carlos
Madrid, Spain

Charles C. Miller III PhD
Department of Cardiothoracic and Vascular Surgery
The University of Texas Medical School at Houston
Memorial Hermann Heart and Vascular Institute
Houston, TX, USA

Michael de Moor MBBCh, FACC, FSCAI
Pediatric Cardiology Division
Floating Hospital for Children
Tufts University Medical Center
Boston, MA, USA

Anton Moritz MD, PhD
J.W. Goethe University
Frankfurt/Main, Germany

Sabareesh K. Natarajan MD, MS
Endovascular Research Fellow and Voluntary Assistant Professor, Health Sciences
Department of Neurosurgery and Toshiba Stroke Research Center
University at Buffalo
State University of New York
Buffalo, NY, USA

Christoph A. Nienaber MD, PhD
Professor of Medicine Chair, Division of Cardiology
University Hospital Rostock
Rostock, Germany

Uwe Nixdorff MD, FESC
Professor of Medicine
European Prevention Center
Duisburg, Germany

Sean O'Donnell MD, FACS
Director of Vascular and Endovascular Surgery
Center for Vascular Care
Washington Hospital Center
Washington, DC, USA

Yoshinobu Onuma MD
Thoraxcenter
Erasmus Medical Center
Rotterdam, The Netherlands

Adytia Pandey MD
Assistant Professor, Neurosurgery
University of Michigan
Michigan, USA

Natesa G. Pandian MD
Professor of Medicine
Center for Cardiovascular Imaging
Tufts University Medical Center
Boston, MA, USA

Patrick Peeters MD
Department of Cardiovascular and Thoracic Surgery
Imelda Hospital
Bonheiden, Belgium

Milind S. Phadke MD
Senior Registrar, Department of Cardiology
Seth GS Medical College and KEM Hospital
Mumbai, India

Tina L. Pinto Slottow MD
Division of Cardiology
Washington Hospital Center
Washington, DC, USA

Shakeel A. Qureshi MD
Department of Congenital Heart Disease
Evelina Children's Hospital
London, UK

Jörg Radermacher MD
Professor of Medicine
Head, Department of Nephrology
Johannes Wesling Klinikum Minden
Minden, Germany

Steve Ramcharitar BM BCh DPhil MRCP
Thoraxcenter
Erasmus Medical Center
Rotterdam, The Netherlands

Tim C. Rehders MD
Department of Medicine
Division of Cardiology at the University Hospital Rostock
Rostock School of Medicine
Rostock, Germany

Wolfgang Roggendorf MD
Professor of Medicine
Department of Neuropathology
Institute of Pathology
University of Würzburg
Würzburg, Germany

Dieter S. Ropers MD, FESC, FACC
Assistant Professor of Medicine
Department of Cardiology
University of Erlangen
Erlangen, Germany

Hazim J. Safi MD
Department of Cardiothoracic and Vascular Surgery
The University of Texas at Houston Medical School
Memorial Hermann Heart and Vascular Institute
Houston, TX, USA

Frederick St. Goar MD, FACC, FSCAI
Evanston Northwestern Health Care
Cardiovascular Institute
Mt View, CA, USA

Volker Schächinger MD
Professor of Medicine
Head, Department of Cardiology
Klinikum Fulda
Fulda, Germany

Hans-Joachim Schäfers MD, PhD
Professor of Surgery
Chair, Department of Thoracic and Cardiovascular Surgery
University Hospital of Saarland
Homburg/Saar, Germany

Hartzell V. Schaff MD
Professor of Surgery
Chair, Department of Cardiovascular Surgery
Mayo Clinic
Rochester, MN, USA

Dierk Scheinert MD
Professor of Medicine
Clinical Director of the Parkhospital Liepzig
Medical Clinic I, Angiology, Cardiology and Heart Center Leipzig, Department for Angiology
Leipzig, Germany

Andrej Schmidt MD
Parkhospital Leipzig
Medical Clinic I, Angiology, Cardiology and Heart Centre Leipzig, Department for Angiology
Leipzig, Germany

Philipp A. Schnabel MD
Professor of Medicine
Institute of Pathology
University Clinics Heidelberg
Heidelberg, Germany

Juerg Schwitter MD, FESC
Director, Cardiac MR Center of the University Hospital Lausanne—CHUV
Associate Professor, Cardiology Section
Lausanne, Switzerland

Patrick W. Serruys MD, PhD, FESC, FACC
Professor of Medicine
Head, Department of Interventional Cardiology
Thoraxcenter
Erasmus Medical Center
Rotterdam, The Netherlands

Leon D. Shturman MD
Cardiac MR/PET/CT Program
Massachusetts General Hospital
MA, USA

Adnan H. Siddiqui MD PhD
Assistant Professor of Neurosurgery and Radiology
Departments of Neurosurgery and Radiology and Toshiba Stroke Research Center
University at Buffalo, State University of New York
Department of Neurosurgery
Millard Fillmore Gates Hospital, Kaleida Health
Buffalo, NY, USA

Horst Sievert MD, FESC, FACC
Professor of Medicine
Head, Department of Cardiology
Cardiovascular Center Frankfurt
Frankfurt, Germany

Kenneth V. Snyder MD, PhD
Department of Neurosurgery and Toshiba Stroke Research Center
University at Buffalo, State University of New York
Buffalo, NY, USA

Torsten Sommer MD
Professor of Medicine
Head, Department of Radiology
DRK Krankenhaus Neuwied
Neuwied, Germany

Christodoulos Stefanadis MD
Professor of Cardiology
Chair, Department of Cardiology
Hippokration Hospital
Athens Medical School
Athens, Greece

Bradley H. Strauss MD, PhD, FACC
Professor of Cardiology
The Schulich Heart Programme
Sunnybrook Research Institute
Sunnybrook Health Sciences Centre
McLaughlin Centre for Molecular Medicine, University of Toronto
Toronto, Ontario, Canada

Asmir I. Syed MD
Professor of Medicine
Associate Director, Division of Cardiology
Director, Experimental Cardiology
Washington Hospital Center
Washington, DC, USA

Rabih G. Tawk MD
Endovascular Neurosurgery Fellow
Department of Neurosurgery and Toshiba Stroke Research Center
School of Medicine and Biomedical Sciences
University at Buffalo, State University of New York
Department of Neurosurgery
Millard Fillmore Gates Hospital, Kaleida Health
Buffalo, NY, USA

Daniel Thomas MD
Department of Radiology
University Hospital Bonn
Bonn, Germany

John D.R. Thomson MD
Department of Congenital Heart Disease
Leeds General Infirmary
Leeds, UK

Konstantinos Toutouzas MD
Department of Cardiology
Hippokration Hospital
Athens Medical School
Athens, Greece

Jurgen Verbist MD
Department of Cardiovascular and Thoracic Surgery
Imelda Hospital
Bonheiden, Belgium

Frank E.G. Vermassen MD, PhD
Professor of Medicine
Department of Vascular Surgery
Ghent University Hospital
Ghent, Belgium

Paul Vermeersch MD
Antwerp Cardiovascular Institute Middelheim
Ziekenhuis Netwerk Antwerpen
Antwerp, Belgium

Erol Veznedaroglu MD
Director, Stroke and Cerebrovascular Center of New Jersey
Chief Cerebrovascular and Endovascular Neurosurgery
Trenton, NJ, USA

Ron Waksman MD, FACC
Professor of Medicine
Associate Director, Division of Cardiology
Director, Experimental Cardiology
Washington Hospital Center
Washington, DC, USA

Arne Warth MD
Institute of Pathology
University Clinics Heidelberg
Germany

John G. Webb MD
Director, Cardiac Catheterization Laboratory
St. Paul's Hospital
McLeod Professor of Heart Valve Intervention
University of British Columbia
Canada

Susan E. Wiegers MD
Cardiovascular Division
Department of Medicine
University of Pennsylvania School of Medicine
Philadelphia, PA, USA

Neil Wilson MB BS DCH FRCP FRCP(CH)
Consultant Paediatric Cardiologist
Director, Paediatric Cardiac Catheter Laboratory
Department of Paediatrics
John Radcliffe Hospital
University of Oxford
Oxford, UK

Nina Wunderlich MD
Department of Cardiology
Cardiovascular Center Frankfurt
Frankfurt, Germany

José Luis Zamorano MD, PhD, FESC
Professor of Medicine
Chair, Cardiovascular Institute
Hospital Clinico San Carlos
Madrid, Spain

Thomas Zeller MD
Professor of Medicine
Head, Department of Angiology
Heart Centre Bad Krozingen
University of Freiburg
Krozingen, Germany

Preface

Since the introduction of percutaneous transluminal coronary angioplasty by Andreas Grüntzig in 1977, interventional cardiology has offered a variety of less invasive approaches for the treatment of cardiovascular disease compared with surgery with less morbidity, but more competitive regarding long-term clinical outcome.

Modalities like percutaneous coronary interventions, percutaneous closure techniques for the treatment of atrial septal defects, and peripheral vascular interventions are widely used as alternatives to the respective surgical procedures. More recently, percutaneous techniques for aortic valve replacement and mitral valve reconstruction have been introduced. By this expansion of indications for catheter-based interventions a traditional domain of cardiovascular surgery is touched.

In the face of the enthusiasm for less invasive treatment modalities by the interventionalists and the skepticism of many surgeons, we believe that interventional and surgical procedures do represent complementary rather than competitive approaches and that the currently available armamentarium has the potential to offer well-tailored management options for the individual patient.

The idea of this textbook is to discuss the potential clinical benefit of interventional versus surgical modalities for adult patients with cardiovascular disease requiring either an interventional or a surgical procedure and in particular for those patients who might be candidates for both strategies. This discussion is based on the detailed description of the individual pathology, pathophysiology, imaging, and clinical outcome which may be required or helpful when comparing the various treatment options.

Thus, *Cardiovascular Interventions in Clinical Practice* represents a new comprehensive concept designed to aid students, residents, general practitioners, cardiologists, neurologists, and surgeons in understanding the potential clinical benefit of both interventional and surgical management on the grounds of the individual pathology and prognosis.

Jürgen Haase
Hans-Joachim Schäfers
Horst Sievert
Ron Waksman

November 2009

1 Septal Defects and Valvular Heart Disease

1 Pathology of Atrial and Ventricular Septal Defects

Siew Yen Ho
Royal Brompton Hospital and Imperial College London, London, UK

Introduction

Congenital deficiencies of the atrial and ventricular septa are among the most common of congenital cardiac lesions. Ventricular septal defects occur in 24–35% while atrial septal defects occur in 4–11% of liveborn babies with congenital heart disease [1]. These defects can occur in isolation, in combination, or in association with many other defects. A ventricular septal defect is an integral part of tetralogy of Fallot, double-outlet ventricles, and common arterial trunk. It is also frequently encountered in association with complete and congenitally corrected transposition, pulmonary atresia, univentricular atrioventricular connections and coarctation, or interruption, of the aortic arch. When occurring in isolation, diagnosis may be delayed, sometimes well into adult life or later decades. In this chapter, we focus on these septal defects occurring as isolated lesions and discuss some of the complicating anomalies. For a better understanding of the anatomy of atrial and ventricular septal defects, it is pertinent to begin with a review of the normal cardiac septum.

Normal septal structures

Atrial septum

A cursory look from the right atrium gives the impression of an extensive septal structure. In particular, anterosuperior to the oval fossa, the seemingly vast expanse of "atrial septum" is the right atrial wall overlying the aortic root (Fig. 1.1a). Sectional cuts demonstrate the septum limited to the floor of the foramen ovale and the muscular rim immediately around it (Fig. 1.1b). The peripheral structures are the infolded right atrial wall anterosuperiorly, superiorly, posteriorly, and inferiorly, and the fibrofatty sandwich of the atrial and ventricular musculature anteroinferiorly [2]. The superior and posterior parts of the rim, often called the "septum secundum," are mainly the infolded right atrial wall between the base of the superior caval vein and the insertion of the right pulmonary veins to the left atrium. This infolding from the epicardial aspect is known to surgeons as "Waterston's groove," through which the left atrium can be accessed without entering the right atrium. Posteroinferiorly, the rim is continuous with the wall of the inferior caval vein. The true septal component is formed by the floor of the foramen ovale ("septum primum"), which functions like a flap valve by closing against the muscular rim in postnatal life when pressure in the left atrium exceeds that in the right atrium (Fig. 1.1c). In the normal heart, the valve is adequate to overlap the muscular rim so that there is no potential for interatrial shunts. The valve is completely adherent to the rim but there is an adhesion gap, or probe patency, in approximately one-fourth of the population, and this provides the potential for right-to-left shunting through the foramen ovale [3–5]. The rim is an infolding of the muscular wall of the right atrium, and the flap valve is a thin sheet of fibromuscular tissue that is usually 0.5–1.5 mm thick. Fatty tissues of the interatrial groove fill the epicardial side of the fold of the muscular rim. The extent of fatty tissue varies, and when it appears excessive in the normal heart it can give the erroneous impression of lipomatous septal hypertrophy. In young adults, the upper limit of normal fat deposit is defined as 1.5 cm in the transverse dimension on echocardiography [6].

Ventricular septum

In the majority of hearts, the right ventricle is in its anticipated location relative to the left ventricle. When the heart is seen from the front, there is considerable overlapping of the ventricular chambers. The anteriorly situated right ventricle curves over the left ventricle such that the right ventricular outflow tract passes cephalad and a little leftward, crossing over the rightward-directed left ventricular outflow tract (Fig. 1.2a and b). The ventricular septum looks very different when viewed from the right and left ventricular aspects. Significantly, the inlet part on the right side is covered over by the septal leaflet of the tricuspid valve, whereas the corresponding part on the left side borders the aortic outflow tract and is devoid of septal attachments to the

Cardiovascular Interventions in Clinical Practice. Edited by Jürgen Haase, Hans-Joachim Schäfers, Horst Sievert and Ron Waksman.

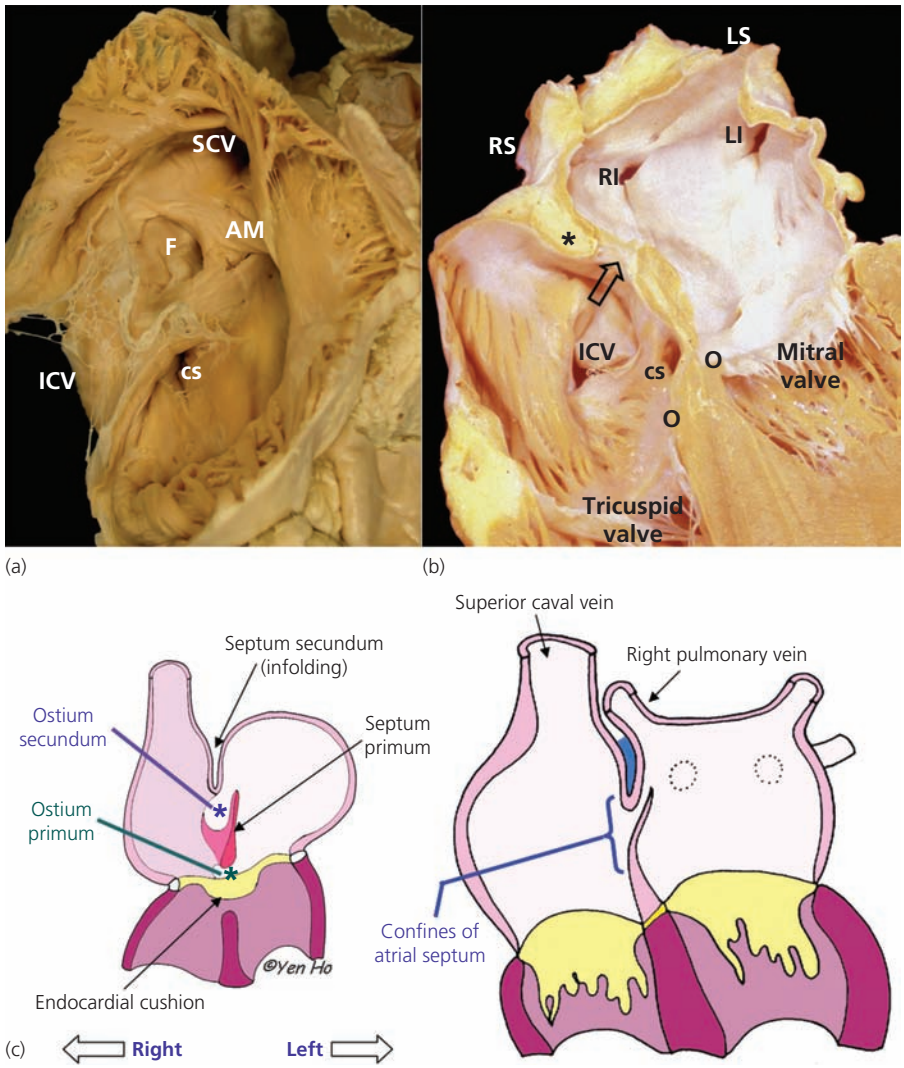

Figure 1.1 (a) The right atrium opened and displayed in right anterior oblique orientation to show the septal aspect *en face*. The oval fossa (F) is surrounded by a muscular rim. The anterior component of the rim extends to the anterior wall lying just behind the aorta (aortic mound; AM). In this heart, the eustachian valve guarding the entrance of the inferior caval vein (ICV) is like a fishnet (Chiari network). (b) A four-chamber cut of a heart shows the atrial septum in profile. The flap valve (open arrow) is thin. The infolding of the right atrial wall enclosing epicardial fat (asterisk) is well seen in this section. The circles mark the offset attachments of the mitral and tricuspid valves. (c) These diagrams represent the change from embryonic to definitive pattern at the atrial septum. The infolded septum secundum with epicardial fat (blue shape) is shown on the right-hand panel. cs, Coronary sinus; LI, LS, RI, and RS, orifices of the pulmonary veins (left inferior, left superior, right inferior, right superior); SCV, superior caval vein.

mitral valve (Fig. 1.2c and d). This is because the acute angulation between inflow and outflow tracts in the left ventricle places the outflow tract between the septum and the "anterior" leaflet of the mitral valve. The septal attachment of the mitral valve is confined to the hinge line (also known as the annulus) of its leaflets, and this is seen only in the posteroinferior parts of the left ventricle close to the cardiac crux. The simulated echocardiographic four-chamber section displays the difference in levels of attachments of the hinge lines of the mitral and tricuspid valves at the septum (Fig. 1.1b). This offset arrangement between the two valves results in a part of the muscular ventricular septum being situated between the right atrium and the left ventricle. Although previously termed the muscular atrioventricular septum, its composition is a sandwich of right atrial wall on one side, crest of the muscular ventricular septum on the other, with intervening fibrofatty tissue from the inferior atrioventricular groove, which ingresses from the epicardium at the crux of the heart. Adjoining the "sandwich" anterosuperiorly is the central fibrous body together with the membranous component of the cardiac septum. The central fibrous body contains the penetrating bundle of His. Its continuation, the atrioventricular conduction bundle, is sandwiched between the crest of the muscular septum and the membranous septum (Fig. 1.3a). This feature is particularly relevant when considering holes in the vicinity of the membranous septum (Fig. 1.3b). The hinge line of the tricuspid valve crosses the membranous septum, effectively dividing it into atrioventricular and interventricular components (Fig. 1.3a). Viewed from the left ventricular aspect, the membranous septum is adjacent to the aortic valve. It adjoins the interleaflet fibrous triangle that lies in between the right and the noncoronary leaflets. Thus, the landmark for the course of the atrioventricular conduction bundle is the septal area between the

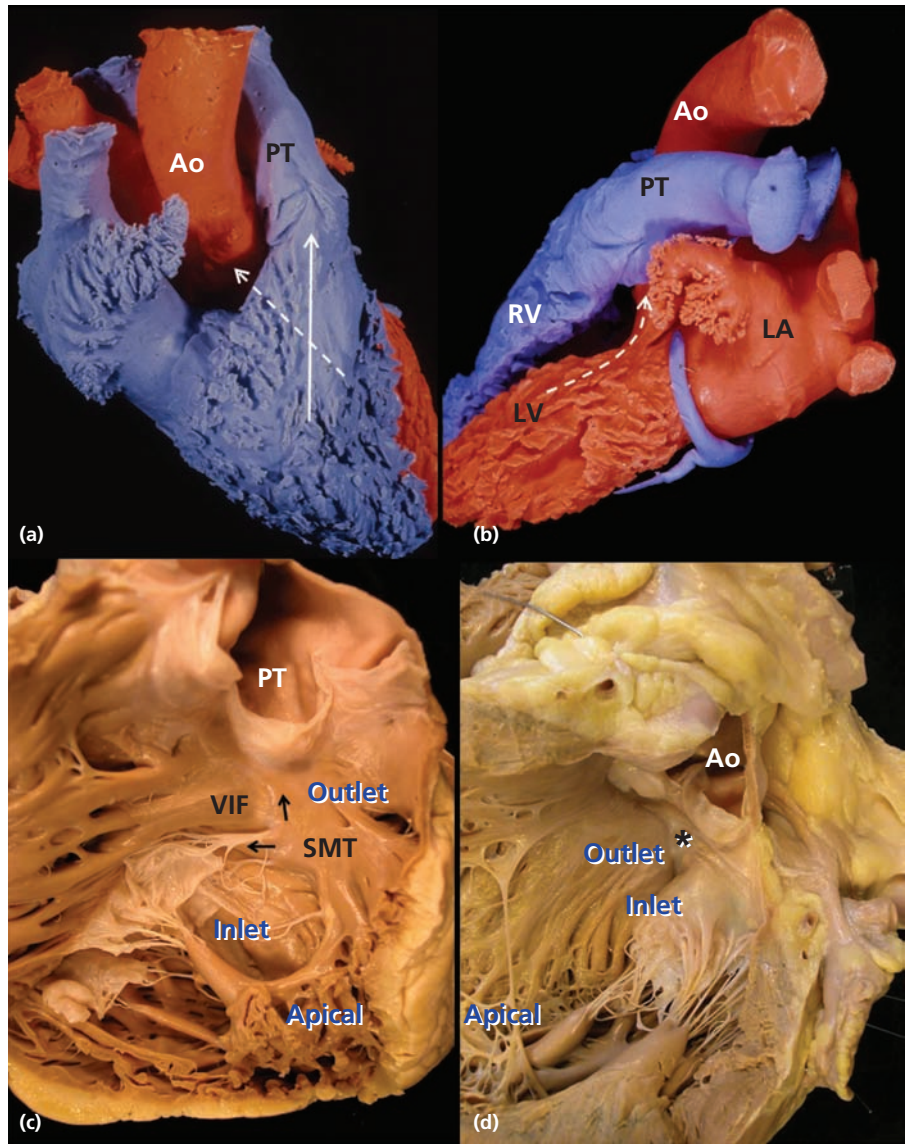

Figure 1.2 (a) This endocast of a normal heart viewed from the front shows the right ventricular outflow tract (solid arrow) crossing over the left ventricular outflow tract (broken arrow). (Note that the pulmonary valve is at a higher level than the aortic valve.) (b) The endocast viewed from the left side shows the relationship of the left ventricular outflow tract (broken arrow) to that of the right. The right ventricle is opened to show the septum and the three portions of the ventricle. (c) The limbs (arrows) of the septomarginal trabeculation (SMT) cradle the ventriculoinfundibular fold (VIF). (d) Dissection into the left ventricular outflow tract shows the proximity of the inlet and outlet portions. The asterisk marks the membranous septum. Ao, aorta; LA, left atrium; LV, left ventricle; PT, pulmonary trunk; RV, right ventricle.

right and noncoronary aortic sinuses. From there, the atrioventricular bundle branches into the right and left bundle branches (Fig. 1.3a). The cord-like right bundle branch passes through the muscular part of the septum to emerge subendocardially close to the insertion of the medial papillary muscle of the tricuspid valve. On the left side of the septum, the left bundle branch descends in the subendocardium to branch into three main radiating and interconnecting fascicles. The branching bundle and the proximal portion of the left bundle branch are, therefore, closely related to the septal aspect of the outflow tract immediately beneath the aortic valve (Fig. 1.3b).

Anterosuperior to the membranous septum is the pulmonary outflow tract exiting from the right ventricle. The musculature anterior to the membranous septum is the supraventricular crest, comprising the ventriculoinfundibular fold and its insertion into the septomarginal trabeculation at the septum (Fig. 1.2c). The septomarginal trabeculation is a characteristic muscle band looking like a tree trunk flattened against the ventricular septum in the right ventricle. It branches into two limbs that cradle the ventriculoinfundibular fold. One limb points anterosuperiorly to blend into the musculature of the subpulmonary infundibulum. The other limb points posteroinferiorly, and it is from this limb that the medial papillary muscle (also known as the conal muscle or muscle of Lancisi) arises to support the anteroseptal commissure of the tricuspid valve. The distal part of the septomarginal trabeculation extends into the moderator band that crosses the right ventricular cavity. The apical portion of the right ventricle bears coarse trabeculations that can obscure the presence of muscular septal defects.

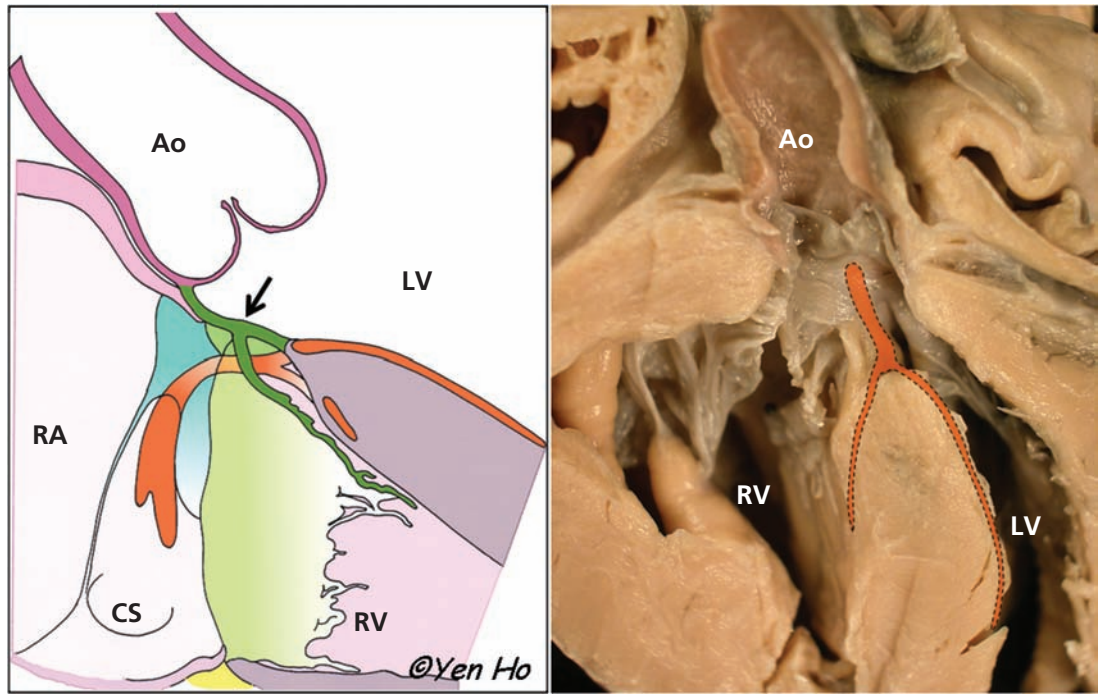

Figure 1.3 (a) Location of the atrioventricular conduction system (orange) in a normal heart. The atrioventricular conduction bundle penetrates through the central fibrous body to pass between the membranous septum and the crest of the ventricular septum, and continues as the branching bundle. The membranous septum (arrow) is crossed by the hinge line of the tricuspid valve. (b) Longitudinal cut through a heart with a perimembranous ventricular septal defect has the atrioventricular conduction bundle (orange shape) superimposed to show the bundle emerging from the area of tricuspid–aortic–mitral valvar fibrous continuity and the close relationship between the bundle and the margin of the septal defect. Ao, aorta; cs, coronary sinus; LV, left ventricle; RA, right atrium; RV, right ventricle.

In the outflow portion of the right ventricle, the conical sleeve of subpulmonary infundibulum is continuous with the ventriculoinfundibular fold. The infundibulum elevates the pulmonary valve away from the septum. Thus, in the normal heart, it is not possible to define a discrete muscular structure equivalent to an outlet septum separating aortic and pulmonary outflow tracts. The outlet septum is expressed in malformations of the outflow tract such as in hearts with Fallot's tetralogy, in which it is an exclusively right ventricular structure.

For convenience in describing the location of holes in the ventricular septum, the right ventricle can be considered as having three portions, although there are no anatomic lines that would allow division of the muscular septum into three parts (Fig. 1.2c). Thus, the inlet portion of the right ventricle is taken to be the portion receiving the tricuspid valve while the outlet portion is the part leading to the semilunar valves, and is mainly musculature proximal to the subpulmonary infundibulum. The remaining portion, the trabecular portion, is the most extensive. Owing to the configuration of the left ventricular inflow and outflow tracts, with the aortic outlet wedged between the septum and the mitral valve, much of the inlet portion of the right ventricle overlaps the outlet portion of the left ventricle (Fig. 1.2d).

Atrial septal defects

Although generally categorized as atrial septal defects (ASDs), some of the defects commonly referred to as ASDs are interatrial communications rather than deficiencies of the atrial septum. This is because the extent of the atrial septum is rather limited when a *septum* is defined as a partition that separates two adjacent chambers, and passage through the septum will not exit the heart (see Atrial septum). Strictly speaking, the septum that separates the two atrial chambers is the valve that is circumscribed by the muscular rim of the foramen ovale (Fig. 1.1a). Defects within this area, usually termed "secundum defects," are true atrial septal defects (Fig. 1.4a). By contrast, sinus venosus defects, coronary sinus defects, and "ostium primum" defects are outside the confines of the true atrial septum although, unequivocally, they permit interatrial shunting (Fig. 1.4a) [3].

Patent foramen ovale

As discussed above, the patent foramen ovale (PFO) is very common. It exists because of an incomplete circumferential adhesion of the *septum primum* (the flap valve of the foramen) to the *septum secundum* (the rim of the fossa). The gap, the last

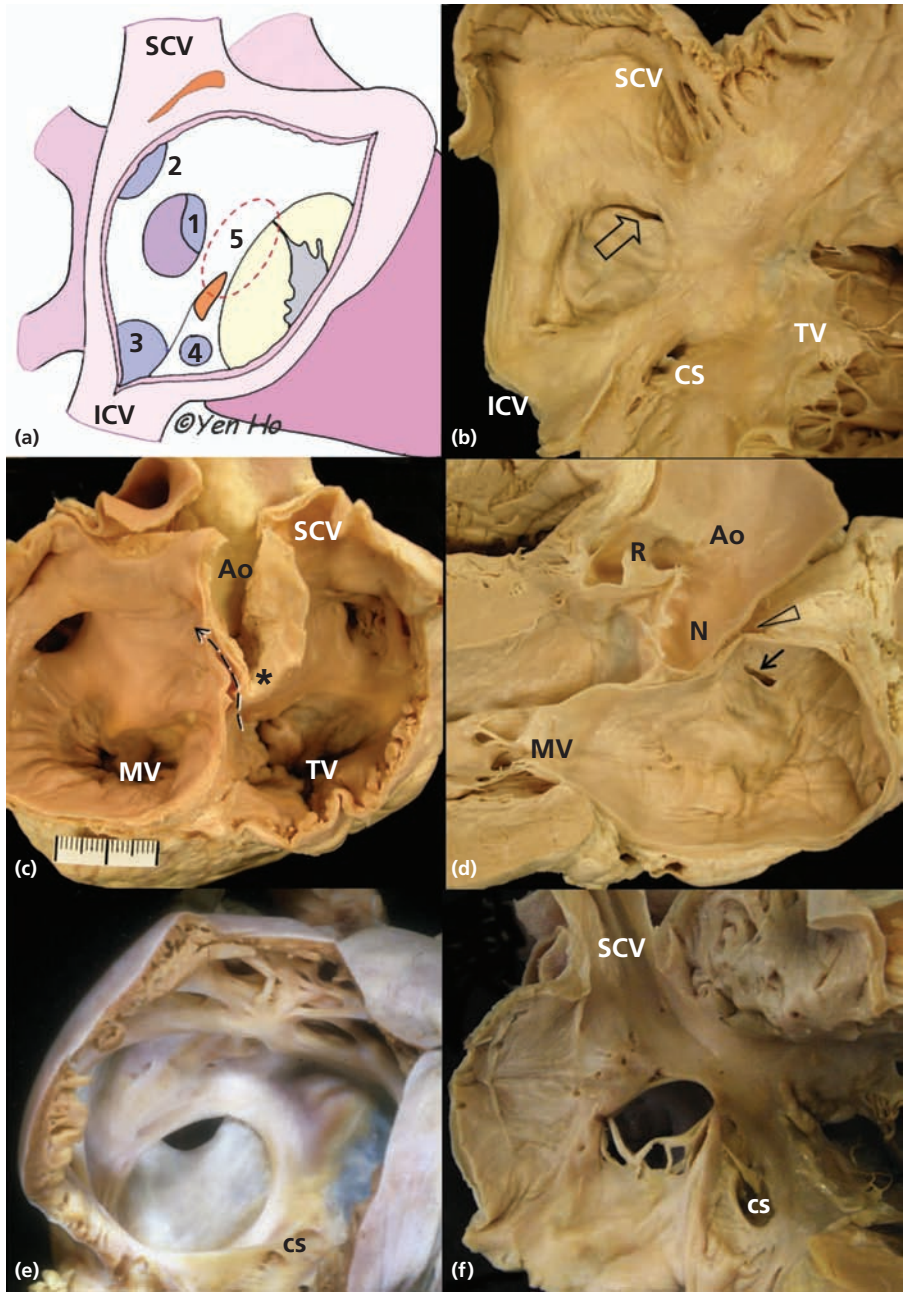

Figure 1.4 Locations of various interatrial communications in the right atrium. (a) The oval fossa defect (1) is the true atrial septal defect. The superior (2) and inferior (3) sinus venosus defects are related to the entrances of the corresponding caval veins. The coronary sinus defect (4) is at the site of the coronary sinus orifice. The atrial component of the atrioventricular septal defect (broken line) is indicated by the number 5. The orange shapes represent the sinus and atrioventricular nodes. (b) The patent foramen ovale (arrow) lies at the anterocephalad margin of the oval fossa. (c) Cut through the atria viewed from behind shows the infolded right atrial wall (asterisk) forming the right margin of the tunnel-like patent foramen ovale (arrow). (Note the aortic root emerging immediately anteriorly.) (d) Long-axis cut through the left heart shows the proximity of the exit (arrow) of the patent foramen ovale to the anterior wall of the left atrium. This part of the atrial wall can be exceedingly thin and it borders the transverse pericardial sinus (triangle) and the noncoronary aortic sinus (N). (e) Right atrial view shows an oval-shaped defect in the atrial septum owing to deficiency of the flap valve. (f) The valve of the oval fossa is lacking and only a few strands remain in the fossa. Ao, aorta; cs, coronary sinus; ICV, inferior caval vein; LV, left ventricle; MV, mitral valve; PT, pulmonary trunk; R, right coronary aortic sinus; SCV, superior caval vein; TV, tricuspid valve.

part of the valve to become adherent, is located at the anterocephalad margin of the rim (if viewing the right atrium in a simulated right anterior oblique projection; Fig. 1.4b). The adhesion gap leaves a slit-like tunnel that allows a probe to be passed obliquely from the right atrium into the left atrium in approximately 25% of cadaver hearts. The length of the tunnel depends on the extent of overlap between the flap valve and the rim [7,8]. In the left atrium the exit site of the probe is at the crescentic margin of the flap valve, and this is closely related to the anterior wall of the left atrium (Fig. 1.4c). This part of the wall can be exceedingly thin, and perforations can lead to the transverse pericardial sinus and the aortic root (Fig. 1.4c and d).

Morphologically, there are two forms of PFO [7]. The first is the valve-competent form in which, under normal circumstances, the valve is large enough to overlap the muscular rim, much like a door closing against a door frame. Although forming a perfect seal, some of these valves are aneurysmal in appearance and bow into the right and left atrial chambers with the respiratory phases. The second form is the

valve-incompetent form, which probably results from stretching of the muscular rim in atrial dilation and/or retraction of the aneurysmal valve, allowing the flap valve to herniate markedly leftward or rightward, reducing the extent of overlap. It is arguable whether this form is due to deficiency of valvar tissues and is a true defect of the oval fossa ("secundum defect").

Defects within the oval fossa

Usually these so-called "secundum" defects are located at the site of the embryonic "ostium secundum" rather than a deficiency of the "septum secundum" since the septum secundum is largely the infolded right atrial wall. Deficiencies, perforations, or complete absence of the valve guarding the foramen ovale (the embryonic "septum primum") are the most common types of interatrial communications with a spectrum of sizes. The simplest form is one resulting from the valve being too small to overlap the muscular rim and so leaving an oval-shaped aperture between the rim and the edge of the valve (Fig. 1.4e). This form is most amenable to transcatheter repair providing there are adequate muscular borders without impinging upon the orifices of the pulmonary veins, the atrioventricular valves, the caval veins, or the coronary sinus [9–11]. Even so, the location of the valve is variable [9]. In some cases, it may be more anteriorly situated or more posteriorly situated. The valve itself may be perforated with single or multiple fenestrations. Sometimes, it appears like a net or is represented by a filigreed remnant (Fig. 1.4f).

When the valve is completely absent, or nearly completely absent, the defect is the hole surrounded by the muscular rim of the fossa. If the anterior rim is deficient, it is worth bearing in mind the proximity of the anterior margin to the transverse sinus and the aortic root. The right coronary and noncoronary aortic sinuses are in the immediate neighborhood. A deficient posterior rim reduces the distance to the orifices of the right pulmonary veins and also increases the proximity to the epicardium due to effacement of the infolding. Occasionally, the defect may extend toward the inferior caval vein or toward the atrioventricular junction. In the case of the latter situation, the distance of the defect from the annular attachment of the mitral valve may become reduced, increasing the risk of damaging the mitral valve during device closure. Although defects in the oval fossa do not alter the basic disposition of the sinus and atrioventricular nodes of the conduction system, these very large defects will reduce the distances between the margin of the defects and the atrioventricular node or the orifice of the coronary sinus.

In cases associated with persistent left superior caval vein draining into the coronary sinus, the coronary sinus is usually enlarged. In these cases, the muscular margin between the coronary sinus orifice and the defect needs to be evaluated carefully. Cases of successful device closure without obstructing coronary venous return have been reported [11].

Sinus venosus defects

These defects are usually located in the mouth of the superior caval vein and described as superior sinus venosus defects. The inferior sinus venosus defects are related to the inferior caval vein and are far less common. The key feature of sinus venosus defects is that they exist outside the confines of the true atrial septum (see Atrial septum). This is not to say that they cannot become confluent, or coexist, with deficiency of the oval fossa.

In the case of a superior sinus venosus defect, the mouth of the superior caval vein typically overrides the atrial septum above the superior rim of the oval fossa (Fig. 1.4a) [12]. Anomalous insertion of the right pulmonary veins into the wall of the superior caval vein is usual in this situation. The defect, therefore, has a well-defined inferior border, the superior rim of the oval fossa, which encloses epicardial fat. Roofing the defect is the overriding caval vein. Owing to the lack of a superior rim for anchorage, currently available devices for closing atrial septal defects are unsuitable. Surgical repair of this defect should take account of potential obstruction to the superior caval pathway following restoration of pulmonary venous return to the left atrium. Also at risk is the sinus node and its arterial supply should there be the need to widen the cavoatrial junction [13].

Sinus venosus defects related to the mouth of the inferior caval vein have similar features to those of superior sinus venosus defects. In the inferior position, the defect's roof is delineated by the posteroinferior rim of the oval fossa and the orifice of the inferior caval vein opens to both left and right atria (Fig. 1.4a). The lower right pulmonary vein can attach anomalously to the wall of the inferior caval vein. This type of defect is remote from the anticipated locations of the sinus and atrioventricular nodes but it lacks an inferior rim for device anchorage.

Coronary sinus defects

Defects termed "coronary sinus defects" cover a spectrum ranging from a hole at the site of the orifice of the coronary sinus and absence of the coronary sinus itself, to a single or multiple fenestrations along the course of the coronary sinus, allowing it to communicate directly with the left atrium. Absence of the wall of the coronary sinus together with the adjoining portion of the left atrial wall results in the deficiency described as unroofing of the coronary sinus [14]. The defect usually leaves the persistent left superior caval vein connecting directly to the left atrium. When existing as a hole at the orifice of the coronary sinus, it may be amenable to device closure [15]. However, closing a large defect at the site of the orifice of the coronary sinus may jeopardize the atrioventricular node because the triangle of Koch becomes foreshortened.

"Ostium primum" defects

This type of defect, although producing an interatrial shunt, is not a true atrial septal defect (Fig. 1.4a). Hearts with

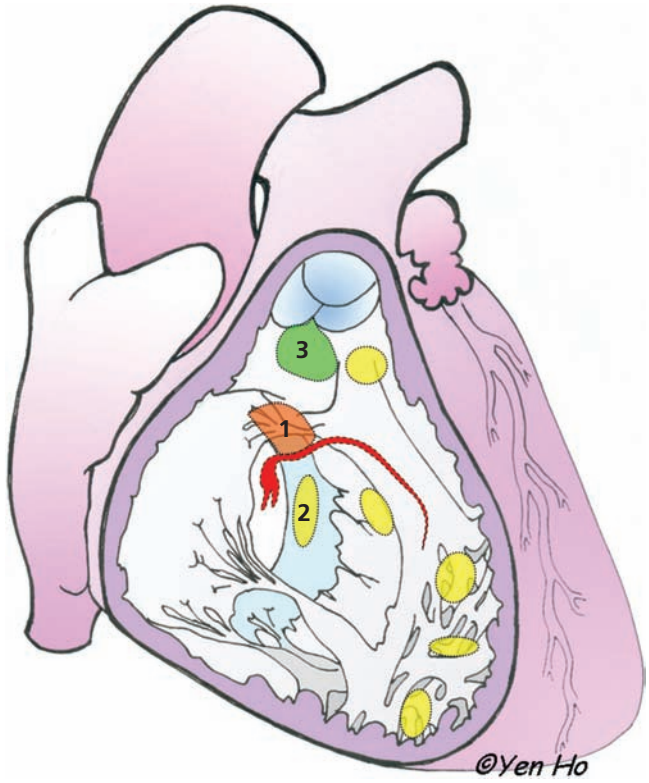

Figure 1.5 Three types of ventricular septal defect as seen from the right ventricle. The atrioventricular conduction bundle (red line) is shown skirting close to the posteroinferior margin of the perimembranous defect (1). By contrast, the bundle is related to the superior margin of a muscular inlet defect (2). Muscular defects can be located anywhere in the muscular septum and are represented by the yellow ovals. The doubly committed and juxtaarterial defect (3) are intimately related to the arterial valves.

this type of defect belong to the spectrum of hearts with atrioventricular septal defect since they have the same characteristic anatomic feature of a common atrioventricular junction [16]. In many cases, the oval fossa is intact and the so-called atrial septal defect exists between the free margin of the atrial septum and the atrial aspect of the conjoined leaflets of the atrioventricular valves. The septal component of the left and right atrioventricular junctions are at the same level (lack of offset between the atrioventricular valves). Owing to the valvar leaflets forming a significant part of the margin of the defect and the displaced atrioventricular node and atrioventricular conduction bundle being in the immediate vicinity, it will be exceedingly difficult to close this type of defect using current transcatheter devices without incurring complications.

Ventricular septal defects

This is one of the most common congenital heart malformations. The incidence is much higher when the defect exists in isolation as most require little if any attention. A major determinant of outcome is the size of the defect. The majority become proportionally smaller with time. Spontaneous closure of the defect occurs in up to half of cases recognized in childhood [17,18], and it has been suggested may also occur in adult life. Generally, those who are asymptomatic are likely to have small defects.

This review of the morphology is restricted to isolated ventricular septal defects. For reasons already discussed, the ventricular component of atrioventricular septal defects will not be included. Also excluded are septal defects following myocardial infarction.

Description of ventricular septal defects

Over the decades, there have been many classifications of ventricular septal defects. In more recent decades, however, three main categories of ventricular septal defects are recognized: *perimembranous* (or membranous/infracristal), *muscular* (or trabecular), and *doubly committed and juxtraarterial* (or infundibular/supracristal/subpulmonary) (Fig. 1.5). These descriptions are applicable to defects existing in isolation as well as in association with other malformations. The distinction between perimembranous and muscular septal defects highlights the relationship of the defect's margins to the atrioventricular conduction system [19].

The location of any hole in the septum between ventricles can be described relative to the three portions of the normal right ventricle, i.e., inlet, apical trabecular, and outlet, with the approach by the surgeon usually from the right side of the heart. Furthermore, the size of the defect and any associated misalignment of septal structures need to be considered in any treatment strategy.

Muscular defects

The muscular defect is characterized by having completely muscular borders. Reportedly, it accounts for 5% of all ventricular septal defects, but its true incidence may be considerably higher as small muscular defects tend to close spontaneously. They can be described as being located in the inlet, outlet, or apical trabecular portions of the right ventricle. Muscular defects, especially those in the apical portion, may be multiple, giving the septum a Swiss cheese appearance, but these are rare. The thick right ventricular trabeculations overlying the septum may make it difficult to visualize or approach these defects from the right side. Some defects appear very small on the right ventricular side but actually form a large confluent defect when examined from the left side (Fig. 1.6a and b).

Muscular defects located in the inlet portion may be partially hidden by the septal leaflet of the tricuspid valve. A rim of muscle separates the border of the defect from the hinge of the tricuspid valve, distinguishing it from a perimembranous defect located in the inlet portion (Fig. 1.5). By virtue of its location, the atrioventricular conduction bundle is related to

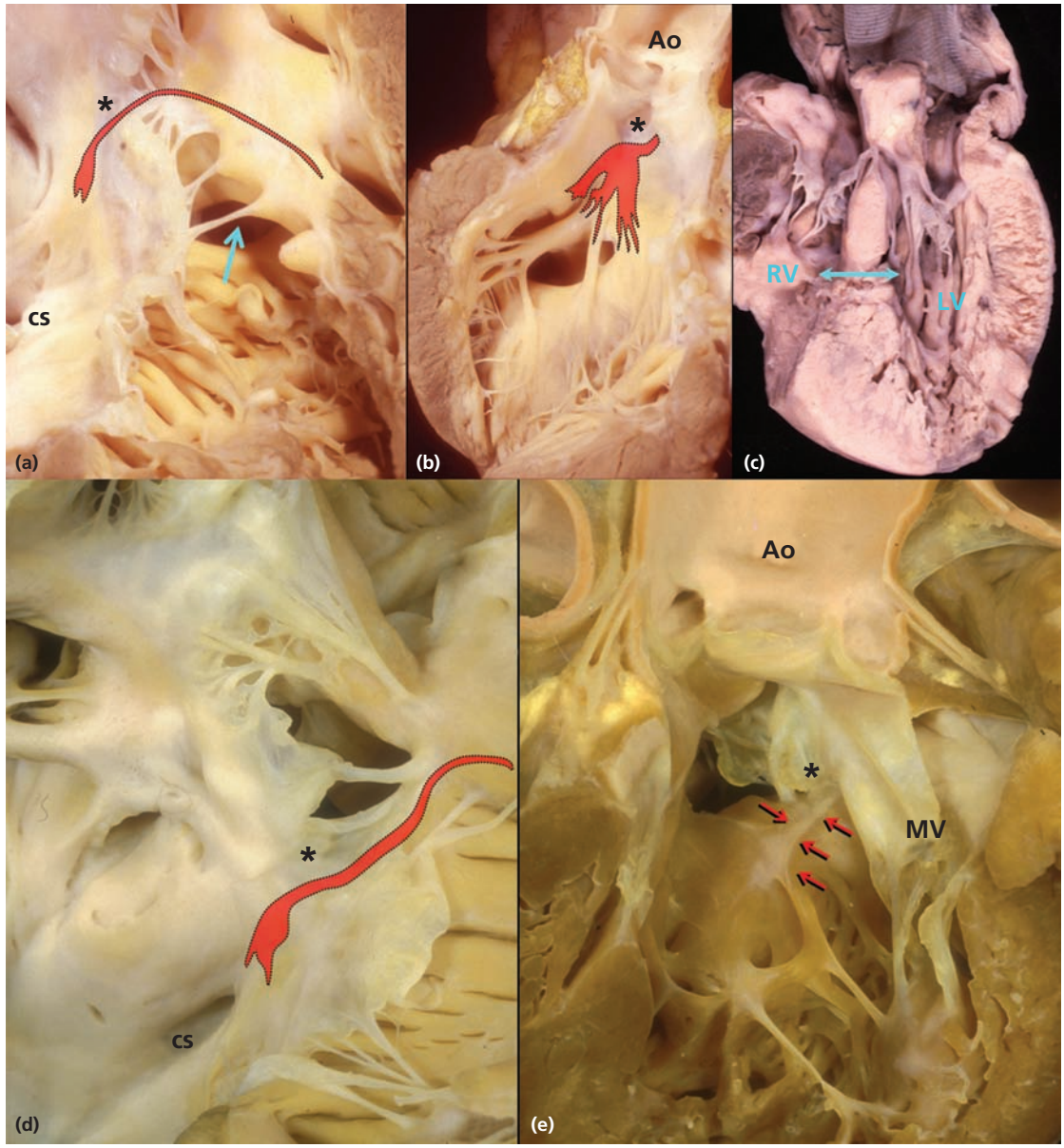

Figure 1.6 (a) Right and (b) left ventricular views of the same heart. The locations of the atrioventricular conduction bundles are superimposed (red) and the membranous septum is marked by an asterisk. The defect (arrow) is small on the right ventricular side but considerably larger on the left side where it is crossed by several muscle bundles. (c) Long-axis cut profiles a muscular defect (arrow) and shows its muscular borders suitable for device closure. (d) Right and (e) left views of the same heart with a perimembranous ventricular septal defect. The defect excavates toward the inlet portion of the right ventricle and is partially covered by the septal leaflet of the tricuspid valve. A remnant of the membranous septum (asterisk) is seen at the posteroinferior border. The atrioventricular node and bundle (red line) pass in this margin. The bundle emerges on the left side and is seen as a white streak (arrows).

the superior margin of the muscular defect. This is in distinct contrast to perimembranous defects (see below). When a muscular inlet defect co-exists with a perimembranous defect, the atrioventricular conduction bundle runs in the muscle bar separating the two defects (Fig. 1.5).

Muscular defects high in the outlet portion are very rare. Seemingly safe from the pulmonary valve, they may be sited close to the aortic valve on the left ventricular side. When the muscular rim in the superior border is narrow, such defects may be difficult to distinguish from doubly committed and juxtaarterial defects (see below).

The majority of muscular defects are not round [20]. They range from being slit-like to the more usual oval shape or D shape (Fig. 1.6a–c). Furthermore, the defects tend to "burrow" through the septum such that their opening on the right side of the septum is offset from that on the left side. In some

cases the opening on one side is larger than on the other side and in others the hole is crossed by muscle bars on one side (Fig. 1.6a and b).

Perimembranous defects

This is the most common type of ventricular septal defect. Being in the environs of the membranous septum, it is related to several important structures. As these defects usually involve a more extensive area than that occupied by the normal membranous septum, they are best described as perimembranous. The key feature of perimembranous defects in all hearts with concordant atrioventricular connections is either a remnant of the membranous septum or fibrous continuity between the atrioventricular valves at the posteroinferior border (Fig. 1.6d and e). It is at this part of the border that the atrioventricular conduction bundle emerges from the central fibrous body to become subendocardial and, in most cases, the branching portion of the bundle appears on the left side of the septal crest.

Perimembranous defects vary in shapes and sizes and can extend toward the inlet, outlet, or apical trabecular portions. Large defects have been described as confluent. In our pathological series [20], the majority of perimembranous defects were oval or round in shape when the septum was viewed *en face* from the right side. When located in the inlet, they are partially, or even entirely, covered over by the septal leaflet of the tricuspid valve (Fig. 1.6d and e). Cords tethering the leaflet usually cross the defect on the right ventricular aspect but in some cases are inserted to the septal crest or to the left side of the septum. In this location, the defect tends to be oval shaped with its long axis parallel to the valvar hinge line. The tricuspid and mitral valves lose their "offset" relationships and their hinge lines form the "roof" of the defect in long-axis echocardiographic sections. Owing to there being a defect, the atrioventricular conduction bundle is displaced more posteroinferiorly than normal, but it is still related to the area of fibrous valvar continuity in the posteroinferior margin of the defect. The medial papillary muscle is located in its anterosuperior border. Perimembranous inlet defects have been described as *atrioventricular canal type* defects [21] but differ in not having the hallmark of a common atrioventricular junction that characterizes atrioventricular septal defects [16].

Perimembranous defects that excavate toward the outlet portion are close to the semilunar valves. Although variable in shape, they tend to be more circular than the other forms of perimembranous defects. In hearts with normal arterial relationships, the aortic valve minimally overrides the septal crest. Aortic, mitral, and tricuspid valvar continuity forms the fibrous posteroinferior border (Fig. 1.3b). Again, it is this fibrous border that harbors the atrioventricular conduction bundle. The medial papillary muscle supporting the tricuspid valve is close to this quadrant of the hole. The distance of the rim of the defect from the conduction bundle depends on the size of the remnant of the membranous septum.

Some perimembranous defects excavate toward the trabecular portion. These tend to be oval or triangular with their long axis directed toward the cardiac apex. In these, the medial papillary muscle is located at the apical quadrant of the defect. Again, the atrioventricular conduction bundle runs in the posteroinferior border. On the left ventricular side of the septum there may be a rim of muscle between the defect and the aortic valve.

Tissue tags adjacent to perimembranous defects can be accessory tissues from the tricuspid valve or the membranous septum. Also described as ventricular septal aneurysms, these are involved in spontaneous closure or diminution in size of the defects [22]. True membranous septal defects are very rare and they are small. Even rarer are defects (described as Gerbode defects) that arise owing to the absence of the atrioventricular component of the membranous septum, resulting in shunting from the left ventricle to the right atrium. Shunts at this level are more often a result of perimembranous defects that are associated with a deficiency in the septal leaflet of the tricuspid valve.

Doubly committed and juxtaarterial defects

These defects account for 5–10% of ventricular septal defects and are more commonly found in the Orient and in Latin America. The feature that characterizes doubly committed and juxtaarterial defects is the lack of muscular separation between the arterial valves in the superior borders. These defects are *roofed* by the pulmonary and aortic valves. Only a fibrous raphe runs between the adjoining valvar leaflets. In some cases, the right coronary leaflet of the aortic valve prolapses into the defect. In many, the posteroinferior margin of doubly committed and juxtaarterial defects is muscular, owing to the fusion between the inferior limb of the septomarginal trabeculation and the ventriculoinfundibular fold. In others, the posteroinferior margin extends to the remnant of the membranous septum and becomes perimembranous. By the nature of their immediate proximity to the semilunar valves, these types of defects are unsuitable for closure using currently available devices. There is hardly any superior margin for safe anchorage without interfering with mobility of the semilunar valves or creating outflow obstruction.

Atrioventricular septal defect

As discussed above, the so-called primum ASD form is unlikely to be suitable for device closure. The form with a common valvar orifice (so-called complete form or atrioventricular canal defect) with both atrial and ventricular defects is also unsuitable. The bridging leaflets of the atrioventricular valve can be compromised. The rarest form that has only a ventricular component of the defect, when carefully selected, may be amenable to device closure. A 4-year-old patient underwent successful implantation of a device with good outcome (Dr. Michael Rigby, personal communication, 2007).

In this child, there was accessory valvar tissue at the margin of the defect.

Malalignment of septal structures

Descriptions of ventricular septal defects are not complete without considering whether the septal components are aligned. Malalignment between atrial and ventricular septa or between components of the muscular ventricular septum have important consequences on the structures in the vicinity of the septal defect. Perhaps the best-known situation of septal malalignment is anterocephalad deviation of the outlet septum in hearts with Fallot's tetralogy. In Fallot, the outlet septum is entirely in the right ventricle and its malalignment produces overriding of the aortic valve as well as subpulmonary stenosis. In contrast, malalignment of the outlet septum into the left ventricular outflow is associated with obstructive lesions of the aortic arch.

Malalignment between atrial and ventricular septa is exemplified by cases with straddling and overriding of the tricuspid valve. Whether existing with isolated ventricular septal defects or with other intracardiac defects, the cardinal feature is that the muscular septum does not extend to the crux of the heart but inserts to the right of the crux. The malalignment results in an abnormally located atrioventricular conduction axis with the atrioventricular node situated in the posterolateral margin of the tricuspid orifice and the bundle penetrating at the point at which the ventricular septum meets the right atrioventricular junction.

Conclusions

A good understanding of the morphological substrates and variations of atrial and ventricular septal defects is particularly relevant in the era of interventional cardiology [10]. An appreciation of the limited extent of the atrial septum helps in distinguishing true atrial septal defects from all other forms of interatrial communications, and also in identifying the ideal site for trans-septal puncture. Interatrial communications that are suitable for transcatheter device closure must be sufficiently remote from the atrioventricular valves, coronary sinus, pulmonary and caval veins, and the aortic root. To minimize the risk of complications, some of these defects, either because of their very large size,or because of their close relationship to these vital structures, require very careful evaluation before considering transcatheter device closure.

Description of ventricular septal defects need not rely on developmental concepts. The categorization described above draws attention to the location of the defect and the proximity of the defect margins to crucial cardiac structures. When considering transcatheter device closure of perimembranous ventricular septal defects, the size of the defect relative to the heart size is important on account of the locations of the aortic valve and the atrioventricular conduction bundle in the immediate vicinity. Ventricular septal defects roofed by the arterial valves and those associated with malalignment of the septal components are unlikely to be suitable for percutaneous device closure without risking damage to adjacent valvar structures.

Acknowledgments

The Cardiac Morphology unit headed by Professor Ho receives funding from the Royal Brompton and Harefield Hospital Charitable Fund.

References

1. Hoffman J.I. (1990) Congenital heart disease: incidence and inheritance. *Pediatr Clin North Am* **37**:25–43.
2. Ho S.Y., Sanchez-Quintana D., Cabrera J.A., *et al*. (1999) Anatomy of the left atrium: implications for radiofrequency ablation of atrial fibrillation. *J Cardiovasc Electrophysiol* **10**:1525–1533.
3. Patten B.M. (1931) The closure of the foramen ovale. *Am J Anat* **48**:19–44.
4. Schroeckenstein R.F., Wasenda G.J., & Edwards J.E. (1972) Valvular competent patent foramen ovale in adults. *Minn Med* **55**:11–13.
5. Hagen P.T., Scholz D.G., & Edwards W.D. (1984) Incidence and size of patent foramen ovale during the first 10 decades of life: an autopsy study of 965 normal hearts. *Mayo Clin Proc* **59**:17–20.
6. Pochis W.T., Saeian K., & Sagar K.B. (1992) Usefulness of transesophageal echocardiography in diagnosing lipomatous hypertrophy of the atrial septum with comparison to transthoracic echocardiography. *Am J Cardiol* **70**:396–398.
7. Ho S.Y., McCarthy K.P., & Rigby M.L. (2003) Morphological features pertinent to interventional closure of patent ovale foramen. *J Interven Cardio*l **16**:1–6.
8. Marshall A.C. & Lock J.E. (2000) Structural and compliant anatomy of the patent foramen ovale in patients undergoing transcatheter closure. *Am Heart J* **140**:303–307.
9. Ferreira S.M.A.G., Ho S.Y., & Anderson R.H. (1992) Morphologic study of defects of the atrial septum within the oval fossa: implications for transcatheter closure of left-to-right shunt. *Br Heart J* **67**:316–320.
10. Rigby M.L. (1999) The era of transcatheter closure of atrial septal defects. *Heart* **81**:227–228.
11. Carlson K.M., Johnston T.A., Jones T.K., & Grifka R.G. (2004) Amplatzer™ septal occluder closure of secundum atrial septal defects in the presence of persistent left superior vena cava to coronary sinus. *Pediatr Cardiol* **25**:686–689.
12. Oliver J.M., Gallego P., Gonzalez A., Dominguez F.J., Aroca A., & Mesa J.M. (2002) Sinus venosus syndrome: atrial septal defect or anomalous venous connection? A multiplane transesophageal approach. *Heart* **88**: 634–638.
13. Busquet J., Fontan F., Anderson R.H., Ho S.Y., & Davies M.J. (1984) The surgical significance of the atrial branches of the coronary arteries. *Int J Cardiol* **6**:223–234.

14. Raghib G., Ruttenberg H.D., Anderson R.C., *et al.* (1965) Termination of left superior vena cava in left atrium, atrial septal defect, and absence of coronary sinus; a developmental complex. *Circulation* **31**:906–918.
15. Di Bernado S., Fasnacht M., & Berger F. (2003) Transcatheter closure of a coronary sinus defect with an Amplatzer septal occluder. *Catheter Cardiovasc Interv* **60**:287–290.
16. Becker A.E. & Anderson R.H. (1982) Atrioventricular septal defects. What's in a name. *J Thorac Cardiovasc Surg* **83**:461–469.
17. Alpert B.S., Mellitis E.D., & Rowe R.D. (1973) Spontaneous closure of small ventricular septal defects; probability rates in the first five years of life. *Am J Dis Child* **125**:194–196.
18. Corone P., Doyen F., Gaudeau S., *et al.* (1997) Natural history of ventricular septal defect. A study involving 790 cases. *Circulation* **55**:908–915.
19. Milo S., Ho S.Y., Wilkinson J.L., & Anderson R.H. (1980) The original anatomy and atrioventricular tissues of hearts with isolated ventricular septal defects. *J Thorac Cardiovasc Surg* **79**:244–255.
20. McCarthy K.P., Leung P.K.C., & Ho S.Y. (2005) Perimembranous and muscular ventricular septal defects—morphology revisited in the era of device closure. *J Interven Cardiol* **18**:507–513.
21. Neufeld H.N., Titus J.L., DuShane J.W., *et al.* (1961) Isolated ventricular septal defect of the persistent common atrioventricular canal type. *Circulation* **23**:685–696.
22. Ramaciotti C., Keren A., & Silverman N.H. (1986) Importance of (perimembranous) ventricular septal aneurysms in the natural history of isolated perimembranous ventricular septal defect. *Am J Cardiol* **57**:268–272.

2 Echocardiography of Atrial and Ventricular Septal Defects

Natesa G. Pandian[1], Antonietta Evangelista[1], Francesco F. Faletra[2], Stefano De Castro[1], Siew Yen Ho[1], Anirban Banerjee[1] & Carey Kimmelstiel[1]

[1]Center for Cardiovascular Imaging, Tufts University Medical Center, Boston, MA, USA
[2]Cardiocentro, Lugano, Switzerland

Introduction

Atrial septal defects (ASDs) and ventricular septal defects (VSDs) represent 10% and 25–40%, respectively, of all congenital heart diseases diagnosed at birth. ASDs, in particular, constitute around 30% of the congenital heart defects diagnosed in adults [1]. Although the primary method of therapy for closure of the ASD and VSD has been surgical repair for many decades, approaches that employ catheter-based devices have emerged as the method of choice for many lesions in recent decades [2]. The development and spread of those new interventional techniques have generated the need for appropriate selection of patients for this therapeutic approach [3]. The purposes of the diagnostic examination in patients with these lesions include detection and delineation of the site, size, and geometry of the defect, recognition of the spatial relationship of the lesion to adjacent structures, assessment of the hemodynamic impact of the lesion, and unmasking of associated lesions. This chapter will review the anatomy, pathophysiology, echocardiographic diagnosis, and treatment of atrial and ventricular septal defects, with emphasis on features that have a bearing on percutaneous interventions for both disorders.

Atrial septal defects

Embryology and anatomy of the atrial septum

At the fourth and fifth weeks of gestation, the division of the atria begins with the formation of the septum primum, creating a temporary communication between the two atria—the ostium primum. Before complete closure of the ostium primum, numerous perforations appear in the superior part of the septum primum. The coalescence of these perforations results in the formation of the ostium secundum. At this point of embryologic development, the superior rim of the atrial septum evolves, formed by extensive infolding of the atrial wall between the venous component of the right atrium and the right pulmonary veins. This, called the septum secundum, overlaps the ostium primum, creating the foramen ovale.

The atrial septum from the right atrial septal surface is formed by the fossa ovalis and its surrounding rim. The rim often appears as thicker or raised muscle that surrounds an oval-shaped depression (the fossa) that is covered over by a thin valve that lies on the left atrial aspect. The fossa ovalis is completely overlapped by its valve, a flap of tissue that is continuous with the left atrial wall. During fetal life, the valve opens leftward, allowing blood to flow from the right atrium into the left atrium through its aperture (foramen ovale). After birth, higher pressure in the left atrium pushes the valve rightward onto its rim, closing the foramen ovale. The fossa ovalis is anatomically closed in about two-thirds of adults as a result of complete adhesion of the valve to its rim. In the remaining one-third it remains patent at the site of the previous foramen ovale. A patent foramen ovale remains a potential source for right-to-left shunt. A redundant valve tissue may form an aneurysm of the fossa ovalis. It is the valve of the fossa ovalis that is the target for trans-septal crossing when interventions are performed. Although the right aspect of the septum is often characterized by the crater-like structure of the fossa ovalis, the atrial septum is relatively featureless when viewed from the left atrium [4].

Pathophysiology and management

Clinical effects of isolated ASDs are usually related to left-to-right shunting. The magnitude of the shunt is related to the size of the defect and to the relative compliance of the left- and right-sided cardiac chambers, and indirectly related to the resistance of the pulmonary and systemic circulation [5]. Approximately 15% of ostium secundum ASDs spontaneously close by 4 years of age. If left untreated, patients with hemodynamically significant ASDs will develop symptoms of right-sided heart failure secondary to pulmonary hypertension (due to the pulmonary vascular obstructive disease caused by increased right-sided flow). Certain types of ASDs (sinus venosus and

Cardiovascular Interventions in Clinical Practice. Edited by Jürgen Haase, Hans-Joachim Schäfers, Horst Sievert and Ron Waksman.

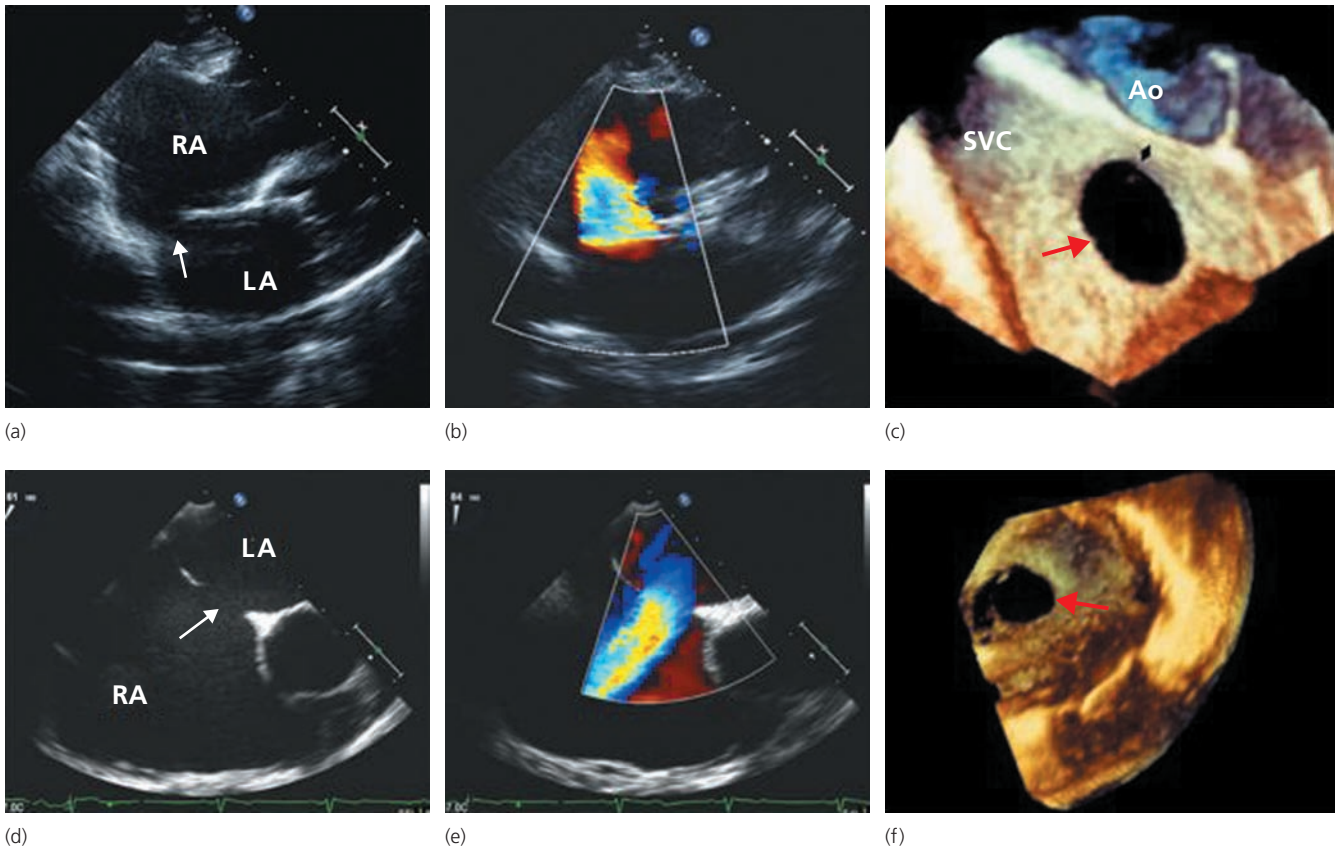

Figure 2.1 2-D and 3-D echocardiographic images of secundum ASDs. (a) A subcostal 2-D echocardiographic image displaying a large ASD. (b) The shunt flow through the defect. (d, e) The defect and shunt flow in TEE recordings. (c, f) 3-D echocardiographic *en face* images of ASDs: (c) the right atrium; (f) the left atrium. The *en face* images are useful in measuring the size of the defect and that of the surrounding rims. RA, right atrium; LA, left atrium; SVC, superior vena cava; Ao, Aorta.

primum varieties) do not close spontaneously. Their location and the presence of concomitant lesions preclude transcatheter closure. Surgery is recommended for patients with these types of ASDs [6]. In patients with patent foramen ovale (PFO) after a cryptogenic stroke, closure of the interatrial communication with surgery or a catheter-delivered device should be considered if the cerebral events are prolonged or recurrent, or if they are followed by residual neurologic deficit [7].

As a general rule, adults with a significant ASD with evidence of right heart dilation should be offered elective closure soon after the diagnosis is established, irrespective of age, whereas in children, device closure is often performed at 5 years of age. Current indications for ASD closure are [8] right atrial and right ventricular dilation, ASD minimum diameter >10 mm, and/or pulmonary to systemic flow ratio (Q_p/Q_s) of >1.5:1.0. Transcatheter device closure of secundum atrial septal defects now represents the standard of care for this abnormality. Indications for catheter closure are the same as for surgical closure, but patient selection criteria are more narrowly defined [9]. Patients in whom the stretched secundum ASD is >36 mm, the atrial septal rims are inadequate (<4–5 mm) to permit stable device deployment, the defect is in close proximity to the atrioventricular valves, the coronary sinus, or the venae cavae, or in whom other cardiac conditions requiring surgical repair are present are usually referred for surgical repair [10].

Echocardiographic anatomy and diagnosis of atrial septal defects

There are four major types of ASDs: ostium secundum, ostium primum, sinus venosus and coronary sinus septal defect (Figs. 2.1 and 2.2). Two- and three-dimensional echocardiography (2-DE and 3-DE) provide direct noninvasive visualization of all types of ASD (Fig. 2.3). Doppler techniques aid in the detection and quantitation of the shunt flow (Fig. 2.3). Although the lesions are identified as interruptions in the linear image of the atrial septum on a 2-D echocardiographic image, 3-DE can display the hole in the septum in *en face* views and allow for the measurement of the geometry of the defect and its rim. The presence of an ASD is generally suspected by indirect echocardiographic findings: enlargement of the right ventricle, septal flattening, and paradoxical motion of the interventricular septum (Fig. 2.3). These findings suggest right ventricular volume overload and represent grounds for suspicion of a defect.

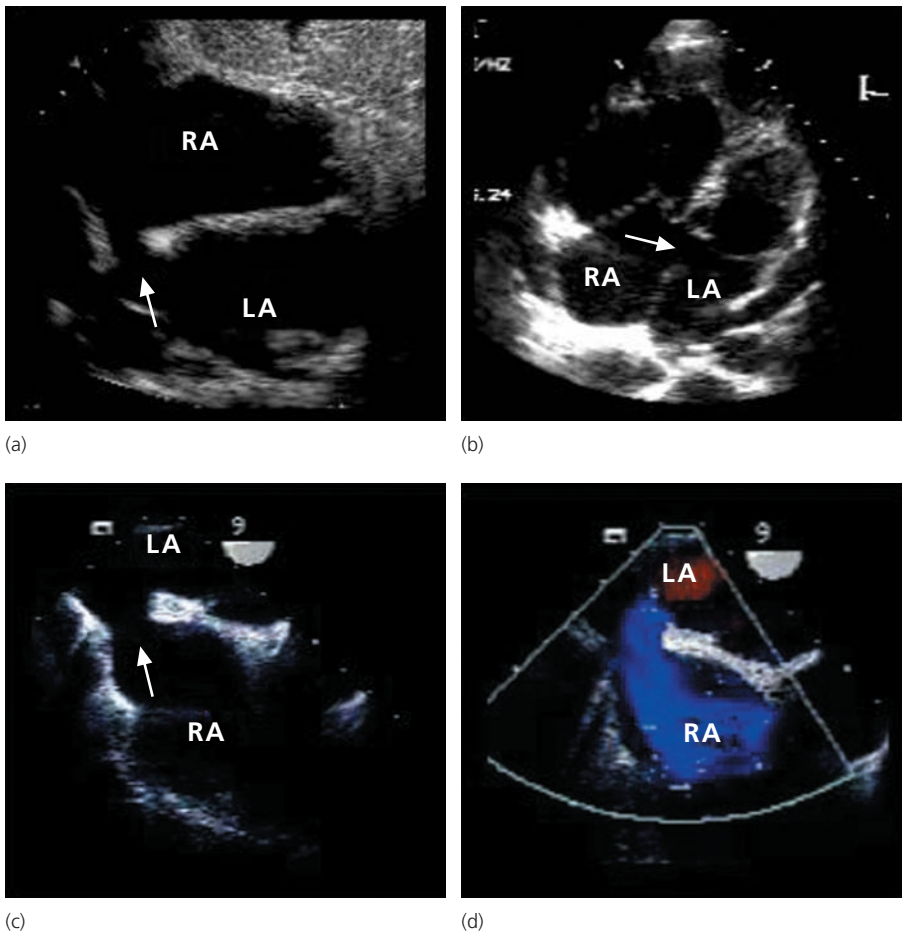

Figure 2.2 Various types of ASDs are shown in these 2-D echocardiographic images. (a) A subcostal transthoracic view showing a sinus venosus type ASD (arrow). (b) An ostium primum defect. (c, d) TEE images of a sinus venosus defect. RA, right atrium; LA, left atrium.

The *ostium secundum* defect, located in the area of the fossa ovalis, is the most common type of ASD, accounting for about 75% of all cases. The shape of the defect varies from circular to oval. Less often, strands of tissue cross the defect, creating a fenestrated appearance that suggests multiple defects. Rarely, a defect can extend posteriorly and inferiorly, approaching the site of inferior vena cava entry into the right atrium. Transthoracic 2-DE views in the parasternal short axis, as well as apical and subcostal four-chamber views, allow for the detection of ASDs. Ostium secundum ASD is visualized in the middle portion of the septum in the fossa ovalis area (Fig. 2.1). Modified views that place the interatrial septum as perpendicular to the imaging plane as possible are often needed to delineate the defect and measure the dimensions. When transthoracic examination is suboptimal, transesophageal echocardiography (TEE) provides crisp definition of the lesion (Fig. 2.1). The ostium secundum defect lies centrally and the sinus venosus more superiorly, with the mouth of the superior vena cava overriding its superior margin. It is important to interrogate the entire atrial septum to ensure that small defects at the margins of the septum are not missed [11].

Color Doppler displays the presence and direction of the shunt flow across the ASD. From transthoracic 2-DE and 3-DE images, the following measurements can be made: dimensions, area and circumference, and the extent of the rim surrounding the defect. 3-DE, particularly by TEE approach, provides excellent images of all four rims of the atrial septum surrounding the ASD. The tissue surrounding the defect is measured as follows: the superior–anterior rim is the distance from the anterior border of the defect to the outer aortic wall closest to the defect; the inferior–anterior rim is from the inferior border of the defect to the tricuspid valve annulus; the superior–posterior rim is between the superior border of the defect to the midpoint of the inlet orifice diameter of the superior vena cava; and the inferior–posterior rim is from the inferior border of the defect to the midpoint of the inlet orifice diameter of the inferior vena cava [12]. These measurements greatly aid in the selection of patients for transcatheter device closure.

Ostium primum defect

The *ostium primum* defect accounts for about 15% of ASDs, and is located in the lower part (or septum primum) of the interatrial septum (Fig. 2.2). This ASD presumably results from failure of the endocardial cushion to close the ostium primum. This is sometimes termed a partial atrioventricular septal defect. Ostium primum defects involve the common

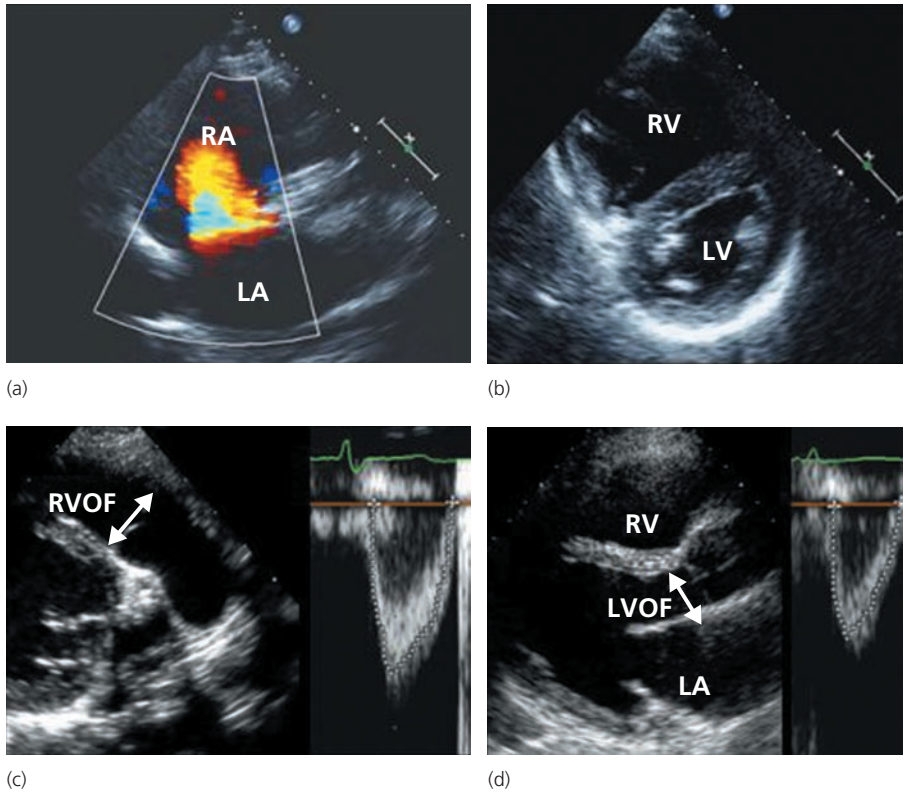

Figure 2.3 (a) A large ASD. (b) A short-axis recording that shows an enlarged right ventricle and flattening of the interventricular septum secondary to volume overload. (c) This image depicts the method of right ventricular outflow dimension measurement and pulsed Doppler recording of flow in that region necessary for quantitation of pulmonary blood flow. (d) Left ventricular outflow tract measurement and flow recording, necessary for quantitation of systemic blood flow. RA, right atrium; LA, left atrium; RV, right ventricle; LV, left ventricle; RVOF, right ventricular outflow tract; LVOF, left ventricular outflow tract.

atrioventricular septum, and are associated with deformity of the alignment of the atrioventricular valves and often with defects of the adjacent interventricular septum. One diagnostic hallmark of the disorder is the absence of the inferior part of the atrial septum (septum primum), which is adjacent to the atrioventricular valves. In contrast to secundum defects, primum defects are more easily visualized from the apical as well as the subcostal approach, with atrioventricular valve tissue forming their lower margin, and the secundum septum forming their upper margin. Ostium primum defects most commonly coexist with a cleft in the anterior leaflet of the mitral valve. Parasternal short-axis 2-D imaging displays a cleft as a gap in the anterior leaflet. The whole span of the cleft is better seen on a 3-D image. Color Doppler often shows a mitral regurgitation jet in various views.

Sinus venosus defect

The *sinus venosus* defect, which accounts for 10% of ASDs, usually involves the superior interatrial septum near the superior vena cava (SVC), and is almost always accompanied by partial anomalous pulmonary venous connection of the right upper pulmonary vein. Less commonly, the defect may occur at the junction of the right atrium and inferior vena cava (IVC) and be associated with an anomalous connection of the right lower pulmonary vein to the IVC. Sinus venosus defects may be difficult to detect by transthoracic 2-DE as they are located superiorly in the interatrial septum near its junction with the superior vena cava. Often nonconventional views should be attempted to image the superior portion of the septum (Fig. 2.2). With TEE, sinus venosus defects, as well as the anomalous pulmonary vein(s), are easily identified. From the upper esophageal window when rotating the imaging plane to about 90°, the distal SVC and the superior atrial septum are visible in their long axis. In the sinus venosus ASD, the SVC often overrides the atrial septum, best seen in the biatrial view.

Coronary sinus defect

Coronary sinus defects are exceedingly rare, difficult to detect with certainty, and are associated with anomalous insertion of a left-sided superior vena cava into the coronary sinus. Modified four-chamber views are necessary to see the coronary sinus and the adjoining atrial septum. In the coronary sinus defect, injection of saline contrast in the left arm reveals transient entry of contrast bubbles into the left atrium, followed by rapid filling of the left ventricle.

All the Doppler modalities form an integral part of the echocardiographic examination of ASDs. Color Doppler displays the shunt flow and direction. From pulsed Doppler recordings of pulmonary and aortic valve flow recordings and 2-D echocardiographic measurement of right ventricle and left ventricle outflow dimensions, the pulmonary (Q_p)–systemic blood flow (Q_s) ratio can be measured by multiplying the cross-sectional area derived from the diameter by the time velocity integral of the flow in the outflow tract (Fig. 2.3). Continuous-wave Doppler provides recordings of tricuspid regurgitation jet velocity from which right ventricle to right atrium systolic pressure gradient is derived. This gradient, added to the estimated right atrium pressure, yields a measurement of right ventricle systolic pressure, and from this posterior–anterior

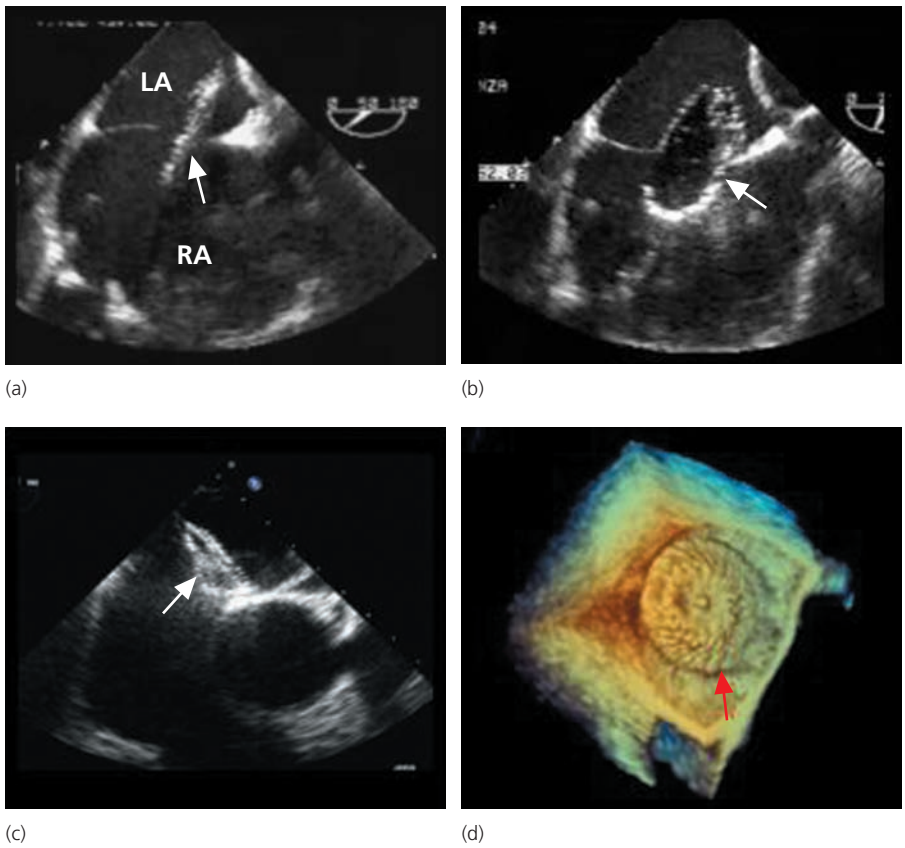

Figure 2.4 Transesophageal echocardiographic images during percutaneous closure of an ASD with an Amplatzer device. (a) A catheter is seen crossing the atrial septum through the ASD. (b) Balloon inflation (arrow) to measure the stretched diameter of the defect. (c) Image after both discs have been deployed (arrow). (d) 3-D echocardiographic image (*en face* view from the left atrium) showing a deployed device. RA, right atrium; LA, left atrium.

systolic pressure. From recordings of pulmonary regurgitation jet, pulmonary artery diastolic pressure can be estimated as well. Although color Doppler images easily reveal the shunt flow of an ASD, contrast echocardiography using agitated saline is helpful in patients with technically suboptimal acoustic windows to unmask a shunt. In the setting of a shunt, microbubbles are seen in the left atrium with systemic venous injection. However, the same finding may be seen in patients with pulmonary arteriovenous fistulae. In the latter, the bubbles arrive in the left atrium after a few heart beats, rather than appearing almost simultaneously in the right and left atria, as is noted in the former condition. An echocardiographic examination is also used to confirm the presence or absence of coexisting disorders, such as mitral valve prolapse, cleft mitral valve, anomalous pulmonary venous drainage, shunt lesions such as a VSD and patent ductus arteriosus (PDA), and stenotic and regurgitant valve lesions.

Patent foramen ovale

The possible role of a PFO in cryptogenic strokes has been well documented [13]. PFO differs from ostium secundum in its tunnel-like morphology. Contrast echocardiography is particularly useful in recognizing PFO, which is too small to be directly seen by conventional transthoracic imaging. Saline contrast examination by TEE coupled with the Valsalva maneuver is a sensitive method to confirm or exclude a PFO.

Guidance during percutaneous closure of atrial septal and patent foramen ovale defects

While transthoracic imaging may provide sufficient guidance during percutaneous closure of ASDs in children, TEE is often needed during such a procedure in adults (Fig. 2.4). Before closure, TEE is used to determine the size of the defect and to measure the ASD rim, as outlined earlier. For closure of ostium secundum ASDs, a 4- to 5-mm rim between the defect and the atrioventricular valves, the superior and inferior caval veins, and the entry of the pulmonary veins into the left atrium [14] is considered to be necessary for the use of closure devices. Additional information is provided about the stretched dimension of the ASD during balloon sizing, the position of the sheath and occluder during and after deployment, the outcome of the procedure after release, the presence of residual shunting, obstruction to systemic or pulmonary venous pathways, and interference with atrioventricular valve function. Under TEE guidance, the left atrial portion of the device is released, and drawn tight. After ensuring that the left atrium side device is well placed and not prolapsing through the defect, the right atrium portion of the device is released. With the closure device in an optimal position, pulling and pushing on the delivery wire or catheter then confirms that the device is secure. After deployment of the device and before disengaging, color Doppler and saline contrast injection are used to interrogate the atrial septum for residual shunt or other secondary defects. 3-DE

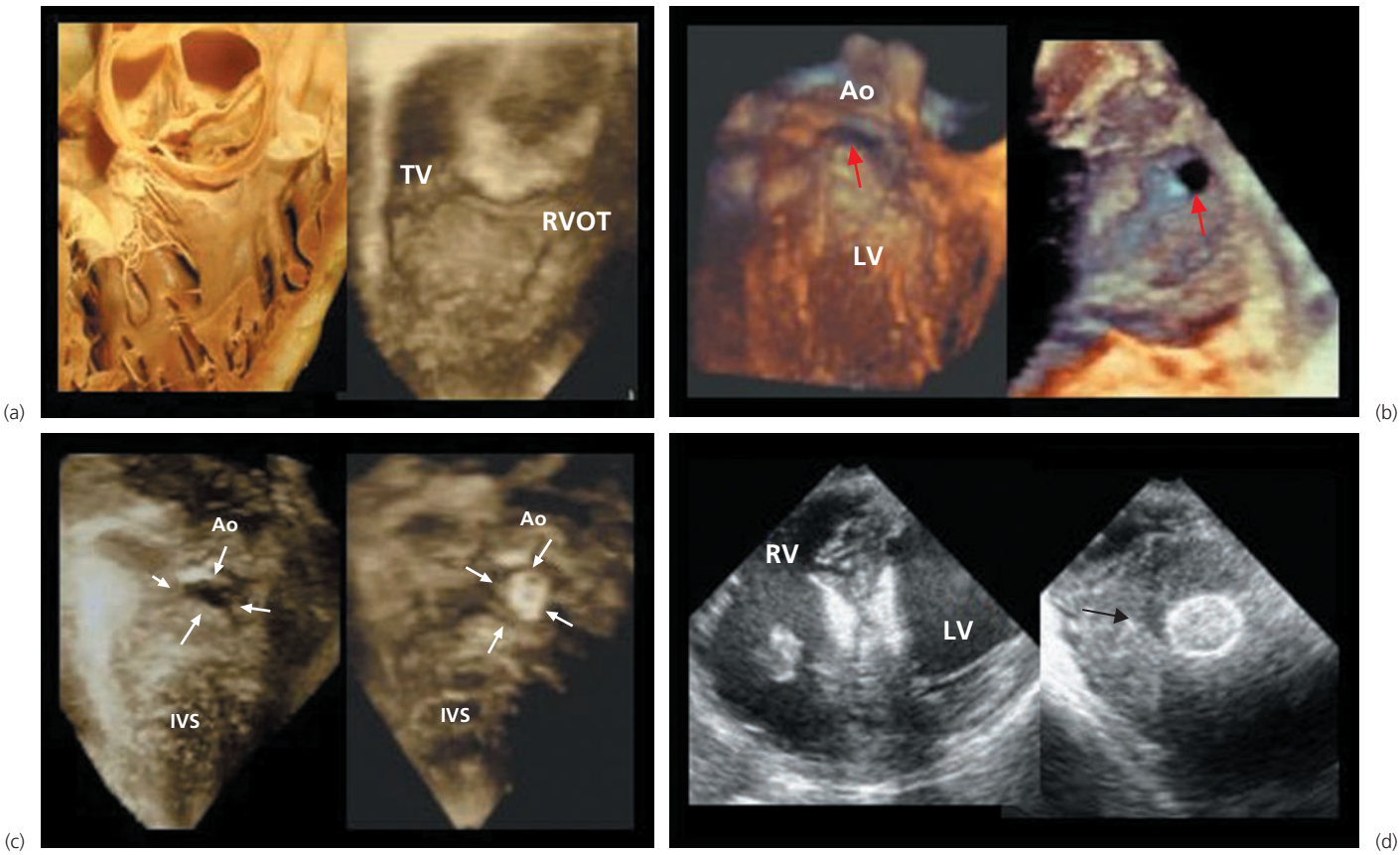

Figure 2.5 (a) Anatomic and 3-D echocardiographic images of a normal interventricular septum seen in an *en face* view from the right ventricle. (b) 3-D echocardiographic images of a membranous VSD (left) and muscular VSD (right). (c) 3-D echocardiographic image of a large VSD before and after closure. (d) An occluder device is seen deployed in a patient with post-infarct VSD; the occluder and a residual defect (arrow) are seen. AO, aortic valve; IVS, interventricular septum; LV, left ventricle; RV, right ventricle; RVOT, right ventricular outflow tract; TV, tricuspid valve.

can also provide valuable information on the mechanism of any residual shunt after device deployment [12,15]. When multiple openings are present, 2-D TEE may fail to detect the exact number of smaller (<2 mm) openings in 25% of cases, but these can be successfully detected by 3-DE. 3-D TEE plays a vital role in preselection of patients with multiple defects for double device closure [16]. Intracardiac echocardiography, imaging with a catheter-based transducer, is another modality helpful in guiding interventions. The advantage of this technique is that the interventionist can perform the procedure whereas TEE requires another operator to introduce and manipulate the TEE probe. However, the imaging plans provided by intracardiac imaging are limited compared with TEE.

Ventricular septal defects

Embryology and anatomy of ventricular septum

The interventricular septum is a highly complex, 3-D structure formed from a number of morphologically distinct subunits. The ventricular septum is formed by contributions from the primitive ventricle and bulbus, the endocardial cushions, and the conal cushions (part of the tissue that develops into the pulmonary artery and aorta). Although the ventricular septum is being formed, the position of the ventricles and the atrioventricular canal region shifts to align each atria and its valve over the correct ventricle. The left ventricle emerges from the primitive left ventricle, and the right ventricle from the bulbus cordis. The major division of the ventricles occurs as a ridge of muscular tissue that folds up into the ventricle and the two sides of the ridge fuse into the muscular or trabecular septum [17]. The remaining part of the ventricular septum is formed by contributions from the endocardial and conal cushion tissue.

The ventricular septum can be divided into two morphological components, the membranous septum and the muscular septum (Fig. 2.5). The membranous septum is small and is located at the base of the heart between the inlet and outlet components of the muscular septum and below the right and noncoronary cusps of the aortic valve. The muscular septum is a nonplanar structure that can be divided into inlet, trabecular, and infundibular components. The inlet portion is inferior–posterior to the membranous septum. It begins at the level of

the atrioventricular valves and ends at their chordal attachments apically. The outlet or infundibular septum separates the right and left ventricular outflow tracts. It is called an "outlet" because it forms the outflow part of the right ventricle, or "infundibular" because it forms the area below the pulmonary artery. Defects occur anywhere along the ventricular septum, and their size and location determine the different types of VSD. When viewed from the right ventricular aspect, VSDs can be described as located at the membranous, inlet, muscular, or outlet portions of the septum. A subarterial (supracristal) VSD is a unique type of VSD in the superior margin of the outlet septum.

Another type of VSD is the acquired VSD, such as posttraumatic ventricular septal rupture or postinfarction VSD (PIVSD) (Fig. 2.5). Despite a reduction in the frequency of PIVSD with the regular use of thrombolysis, the incidence remains as high as 0.2% [18]. Two types of PIVSD exist: simple and complex [19]. Simple ruptures are direct through-and-through defects. Complex ruptures are associated with serpiginous dissection tracts remote from the primary site of tear of the ventricular septum. Complex ruptures occur mostly in the inferior acute myocardial infarction and less in the anterior infarction. Ruptures that involve the inferior–basal portion of the septum are much more likely to be complex than ruptures in all other locations. Septal rupture defects can be either very large or multiple, with the possibility of expanding in size over time. Ventricular septal rupture usually occurs within 1 week after the initial myocardial infarction, but can be a catastrophic complication even within the first 24 h [20].

Pathophysiology and management

The functional disturbance caused by a VSD depends on the magnitude of the shunt. A small VSD with high resistance to flow permits only a small left-to-right shunt, whereas large interventricular communication allows a large left-to-right shunt, if there is no pulmonic stenosis. Quantifying the shunt by the ratio of pulmonary–systemic circulation (Q_p/Q_s) is useful. The severity of pulmonary vascular disease correlates with the size of the shunt. In time, as pulmonary vascular resistance increases, irreversible histologic changes may occur within the pulmonary vascular bed. Untreated, a reversal of the flow occurs, leading to a right-to-left shunt with the development of cyanosis (Eisenmenger complex). The natural history of VSDs encompasses a wide spectrum, ranging from spontaneous closure to congestive cardiac failure and death in early infancy. Muscular VSDs can undergo spontaneous closure as a result of muscular occlusion. Perimembranous defects can close by formation of accessory tissue from the tricuspid valve. Subarterial (supracristal) defects can close by prolapse of the right aortic cusp, sometimes with deleterious effects on the aortic valve. A reduction in the size of the defect by any of these mechanisms results in changes in the hemodynamic significance of the defect. Other defects, such as malalignment ventricular septal defects and the atriovenous canal type or inlet ventricular septal defect, are unlikely to close spontaneously.

Patients with VSD with evidence of significant left ventricular volume overload or progressive aortic valve disease require closure of the defect [21]. Endocarditis is a lifelong risk in unoperated patients and those with residual defects [22]. Proper prophylaxis and periodic follow-up are indicated. Patients with PIVSD are generally in an unstable clinical position, with acute hemodynamic changes that are poorly tolerated because of a reduction in ventricular function. The optimal treatment strategy is still under discussion [23]. Percutaneous closure during the acute phase after the infarction is a high-risk procedure with a high likelihood of failure, as is also the case with surgical repair [24]. Another additional risk involves the theoretical formation of a systemic or pulmonary embolism of fragile parts of necrotic tissue.

Location has been used as an indication for surgical closure regardless of the need for medical management in the case of infundibular defects [25]. Chamber enlargement is another measure of the degree of shunting and may indicate the need for closure. Generally, a change in Q_p/Q_s from 1.5:1.0 to 2:1 [26] or evidence of increased pulmonary arteriolar resistance is an indication for closure. A pulmonary–systemic vascular resistance ratio greater than 0.9:1.0 or pulmonary arteriolar resistance greater than 12 Wood units is regarded as a contraindication to surgery. Multiple "Swiss cheese" defects refractory to medical management may require a palliative pulmonary artery banding procedure.

At the present time, suitable candidates for percutaneous closure are those with a muscular VSD or a residual defect at the patch margins following cardiac surgery, and those who have suffered a myocardial infarction [27] (Fig. 2.5). Because of their close proximity to the aortic and tricuspid valves, perimembranous VSDs are generally considered unsuitable for transcatheter device closure unless there is a contraindication to open heart surgery. Even then, only perimembranous defects opening to the inlet of the right ventricle may be suitable [28]. Other defects unsuitable for device closure include those that are doubly committed and those associated with aortic valve prolapse, a straddling atrioventricular valve, or a distance of less than 4 mm between the border and semilunar or atrioventricular valve [29].

Echocardiographic anatomy and diagnosis of ventricular septal defects

Two- and three-dimensional echocardiographic imaging provides direct noninvasive visualization of all types of ventricular septal defect. Long- and short-axis views and modified apical views can display these defects on 2-DE (Fig. 2.6). A survey of the whole septum from base to apex in various views is necessary to detect and delineate the location, size, and shape of the defects. 3-DE can portray the defect in *en face* projections [30] (Fig. 2.5). Color Doppler imaging aids in the detection by displaying the shunt flow. Continuous-wave Doppler

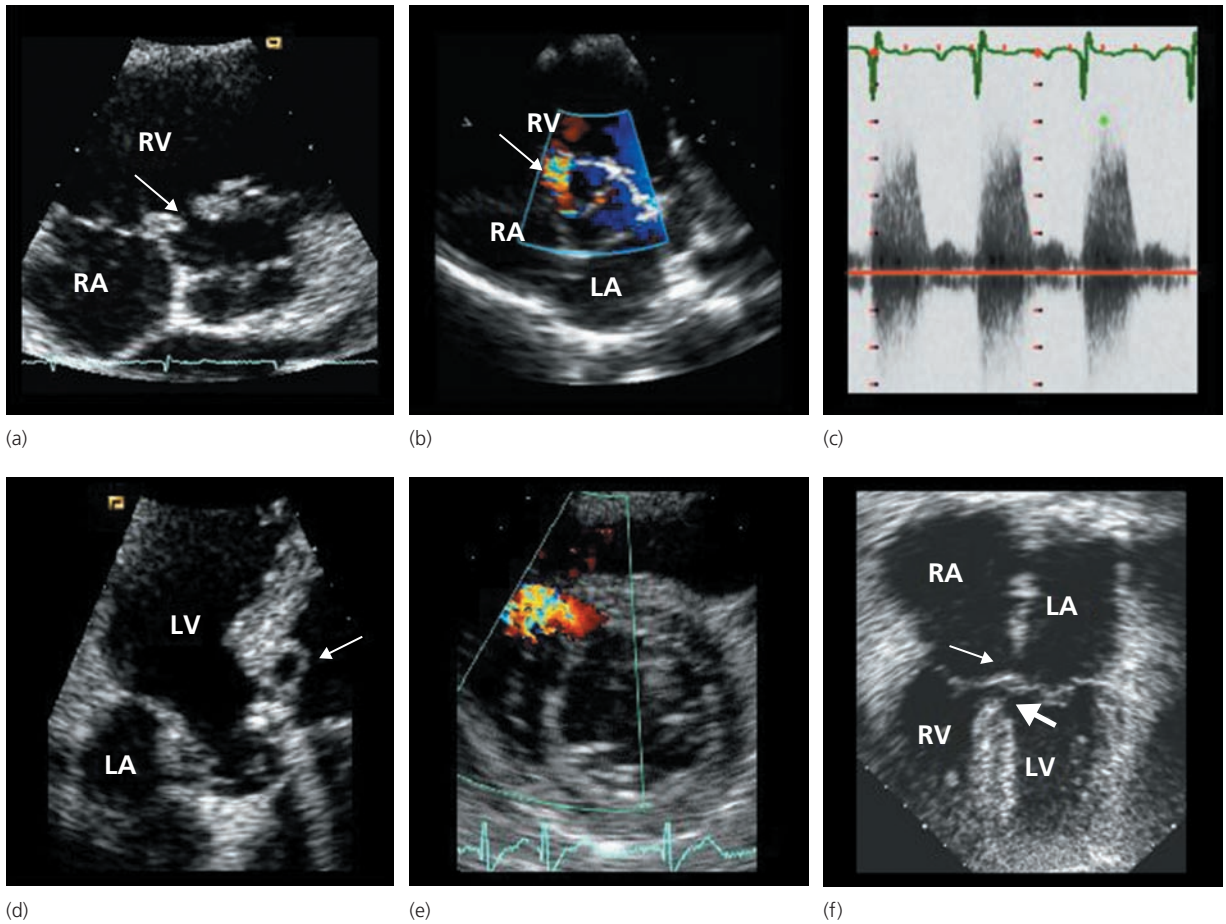

Figure 2.6 Various types of ventricular septal defects are depicted in these 2-D echocardiographic images. (a) A perimembranous VSD in the parasternal short-axis view. (b) Color Doppler displaying a left-to-right shunt through the VSD. (c) Pulsed Doppler recording of the shunt velocity. (d) A VSD and aneurysm of the membranous septum. (e) A muscular type of VSD with shunt flow. (f) Both a VSD (thick arrow) and an ASD (thin arrow) are seen in this patient with the atrioventricular septal defect. RA, right atrium; LA, left atrium; RV, right ventricle; LV, left ventricle.

allows for determination of the gradient between the ventricles (Fig. 2.6).

True defects of the membranous septum are surrounded by fibrous tissue without extension into adjacent muscular septum (Fig. 2.6). Such defects are rare. Defects that involve the membranous septum and extend into one of the three muscular components are called perimembranous VSDs, and are more common. These defects can be associated with the formation of pseudoaneurysm tissue along the right ventricular side of the septum, which can be seen in 2-D and 3-D echocardiographic images. A perimembranous inlet VSD has no muscular rim between the defect and the atrioventricular valve annulus. Defects in the inlet septum can include abnormalities of the tricuspid and mitral valves. Sometimes called common atrioventricular canal defect, they should not be mistaken for the VSD component in hearts with an atrioventricular septal defect. The latter entity has the distinctive morphologic feature of a common atrioventricular junction, which is not seen in hearts with perimembranous inlet VSD. A defect in the trabecular septum is called a muscular VSD if the defect is completely rimmed by muscle (Fig. 2.6). Such defects may be singular and small, and the incidence of spontaneous closure tends to be high; alternatively, they can be multiple with significant hemodynamic effects. In the most severe manifestation, the septum displays a "Swiss cheese" appearance. Color Doppler imaging displays the shunt flow when the septum is scanned in various projections.

Defects in the infundibular septum are called infundibular, outlet, supracristal, conal, conoventricular, subpulmonary, or doubly committed subarterial defects. A deficient infundibular septum may be present with corresponding degrees of misalignment of the infundibular septum and the remainder of the ventricular septum. Although this defect may exist in isolation, it is most frequently associated with other defects such as tetralogy of Fallot.

Three-dimensional echocardiography presents an accurate view of the anatomy of the VSD (Fig. 2.5). Planes that show the VSD from its right aspect reproduce the surgical viewpoint of a right ventriculotomy (right ventricle *en face* view). From these images it is possible to define the morphologic

nature of the margins of the defect, its shape, and the direction in which the defect extends into the ventricular septum. Other anatomic structures such as the tricuspid valve leaflet, the right ventricular outflow tract, and the aortic valve can be displayed in their realistic spatial distribution [31]. Similar to a surgeon's perspective, direct 3-D echocardiographic visualization of certain membranous and muscular VSDs from the right ventricle *en face* view can be obscured by overlying tissue or cardiac structures. In particular, perimembranous VSDs, on the right ventricle side, may be obscured by either tricuspid valve tissue or remnants of the membranous septum; they are best seen from a three-chamber view, which includes the left atrium, left ventricle, and aorta. The perimembranous VSDs are either circular or oval and can consistently be seen immediately below the aortic valve. However, in about 15% of patients, a small, thin rim of tissue, 2 mm in length, is interposed between the aortic valve and superior rim of the defect. From the left ventricle cut plane, certain large perimembranous defects can be seen extending posteriorly to the atrioventricular septum or inferiorly to the muscular septum [30].

The outlet defects are best visualized on parasternal long-axis and short-axis views. In the parasternal short-axis view, they can be differentiated into supracristalis and infracristalis, based on their position above or below the crista supraventricularis. The 3-D echocardiographic *en face* projection from the left side shows doubly committed VSDs to be directly subaortic, albeit slightly more anterior than the typical perimembranous defect. The right ventricle *en face* projection portrays the defects directly subpulmonic, away from the membranous septum and adjacent tricuspid valve. After the diagnosis of an outlet VSD, it is important to thoroughly evaluate these patients for any evidence of aortic valve prolapse (specifically of the right coronary cusp) and for aortic regurgitation. 3-DE not only allows accurate assessment of the VSD size and degree of valve prolapse but also provides enhanced spatial appreciation of the commitment of the defect to both great arteries.

Muscular VSDs can be more difficult to visualize by 3-DE. Like the perimembranous VSDs, the cut plane should be initially oriented parallel to the left ventricle septal surface. However, the cut plane should be then rotated in various directions to better visualize the muscular defects, dependent on their location within the ventricular septum. For example, the cut plane should be rotated to include the aorta to best visualize high muscular defects. A two-chamber view, including only the left atrium and left ventricle, is best used to depict more posterior and/or inferior defects. The 3-D echocardiographic left ventricle *en face* projections provide unobstructed evaluation of the defects, their borders, surrounding structures, and their complex shapes [30]. Defects of the posterior inlet septum are usually best seen from the apical four-chamber and the subcostal view, both of which image the posterior cardiac structures. The septal leaflet of the tricuspid valve may partially obscure these defects, making them appear smaller than they actually are.

Small ventricular septal defects could be difficult to be visualized by 2-D or 3-D imaging alone; color Doppler demonstration of flow through the ventricular septum into the right ventricle aids in the detection of such defects. Doppler estimation of the pressure gradient between the two ventricles is best achieved with the Doppler interrogation beam parallel to the flow from the left to right ventricle. The spectral Doppler signal shows a rapid early systolic rise to a midsystolic peak and rapid late systolic fall; its shape is rather similar to that of atrioventricular valve regurgitation. The maximum velocity of flow through the defect provides a relatively accurate measurement of the pressure difference between the ventricles. The smaller the VSD, the higher is the flow velocity across the defect. The right ventricular pressure can theoretically be estimated by subtracting the interventricular pressure gradient from systolic aortic blood pressure, which is used as a surrogate for left ventricular pressure. A high velocity indicates low right ventricular and pulmonary artery pressure (small VSDs), whereas a low velocity indicates a high right ventricle pressure (usually in the presence of large VSDs). If the jet velocity progressively increases it means that the VSD is likely to close. In patients with Eisenmenger's syndrome, the signal is of low velocity and shows bidirectional flow.

When limitations in image quality prevent evaluation of these aspects of the VSDs by transthoracic echocardiography, transesophageal 2-D and 3-D examinations are useful. From the mid-esophageal window (0°), flexion displays the left ventricular outflow tract and the thin membranous part of the septum. Advancing the probe reveals the muscular/trabecular part of the septum (see muscular VSD), but it may be impossible to fully interrogate the apex in this view. Having performed the 2-D echo sweep, this is repeated using color flow mapping. Although it may be difficult to align the Doppler beam parallel to VSD flow, it is important to look out for turbulence within the right ventricle cavity and a flow convergence zone within the left ventricle cavity. In subarterial (supracristal) VSD and in rarer perimembranous VSDs, TEE is valuable in identifying the prolapse of the right aortic cusp into the defect resulting in aortic regurgitation. Such prolapse may potentially cause permanent damage to the aortic valve leaflets.

Guidance during percutaneous closure of ventricular septal defects

Size and the position and relationship with contiguous cardiac structures are crucial parameters that need to be accurately evaluated for the preoperative description of VSD for planning and performing percutaneous device closure or surgical closure of VSD. Although 2-DE is helpful in the detection of VSD lesions, 3-DE offers a better description of the geometry of VSDs and thus is useful in the selection of patients for surgery or device closure. Because the *en face* projection allows delineation of the shape and of the entire diameters and area, running the images frame by frame enables the dynamic

change of the defect to be observed, and allows the maximum anterior–posterior and superior–inferior diameters and the largest and smallest areas of defect to be measured. This advantage of 3-D imaging is even more apparent when measurements of crescentric and triangular muscular defects are required, and in the case of any VSD with an asymmetric shape. One can also accurately define the location of the VSD in the septum, its relationship with other anatomic structures such as the tricuspid valve, the attachment of the tricuspid valve chordae to the right ventricular wall, the right ventricular outflow tract, and the aortic valve, and the margins of the VSD [32] (Fig. 2.5). Knowledge of the precise relationship to other anatomic landmarks helps avoid complications from device closure such as damage to the aortic or tricuspid valves. The presence of a 2 mm or more rim of tissue between the perimembranous defect and the aortic valve is generally required for device closure of perimembranous VSDs [33], or a distance of more than 4 mm between the border and semilunar or atrioventricular valve for device closure of muscular VSDs [34].

Precise delineation of the size, shape, and position of the VSD helps in appropriate preselection of patients and in planning optimal percutaneous or surgical approaches for defect repair. Criteria for the transcatheter closure of the ventricular septal defects are thought to be single muscular ventricular septal defect (maximal diameter <12 mm and distance >5 mm from the margins of the defect to the mitral valve, aortic valve, and apex) [29]. Balloon sizing of the defect is useful, but the type of closure device selected will depend on many factors, including the preference and experience of the operator, the thickness of the ventricular septum, and the exact morphology of the defect. The preference in the case of solitary defects is to use one of the various Amplatzer occluders (Amplatzer, Plymouth, MN, USA).

The *en face* 3-D echocardiographic view of ventricular septum is particularly useful in patients with PIVSD in deciding whether to use a surgical or percutaneous approach. The location of the PIVSD and the size of the margins of the VSD from the apex or semilunar or atrioventricular valves need to be considered when assessing the apppropriateness of a surgical patch or device closure. In some selected cases, the use of contrast echocardiography can be useful in the detection of PIVSD, in particular for smaller septum rupture or PIVSD with serpiginous aspect. The irregular edges of the PIVSD can be the cause of any residual shunt. The most commonly used device for PIVSD closure is the Amplatzer septal occluder [24] (Fig. 2.5).

VSD closure cannot be performed safely without the use of TEE. This mode of imaging is essential to provide information about the position of the wire, sheath, and occluder during and after deployment, particularly any interference with atrioventricular or semilunar valve function before release. There is a significant risk of a periprocedural hemopericardium which can be recognized immediately. The procedure is technically much more difficult than closure of an ASD. After VSD device closure, the 3-D views can illustrate the geometric profile (flat or mushrooms profile due to oversizing) of the device from both the left and right sidse and can determine if it protrudes in the left or right ventricular outflow tract. Color Doppler imaging is useful to estimate the presence of any residual shunt. Real-time 3-D TEE may reduce radiation exposure from fluoroscopic guidance and also potentially shorten the procedure time for interventions [35].

Conclusion

Various modalities of echocardiography are necessary to recognize atrial and ventricular septal defects, to delineate precisely the size and geometry of the defects as well as the size of their rims, to estimate the shunt flow and pulmonary artery pressures, and to assess the hemodynamic effects on the cardiac chambers. 3-D echocardiography is particularly useful in the selection of patients for surgery and the use of closure devices. 2-D and 3-D TEE have become valuable tools both in the operating room and in the interventional laboratory to guide the corrective procedure, assess the efficacy of closure, and facilitate the immediate detection of complications.

References

1. Dave KS, Pakrashi BC, Woolder GH, *et al.* (1973) Atrial septal defect in adults: clinical and hemodynamic results of surgery. *Am J Cardiol* **31**:7–14.
2. Connelly MS, Webb GD, Sommerville J, *et al.* (1988) Canadian consensus conference on adult congenital heart defects. *Can J Cardiol* **14**:395–452.
3. Konstantinides S, Geibel A, Olschewski M, *et al.* (1995) A comparison of surgical and medical therapy for atrial septal defect in adults. *N Engl J Med* **333**:469–473.
4. Faletra F, Pandian NG, & Ho SY. (2008) The cardiac septum. In: Faletra F, Pandian NG, Ho SY (eds). *Anatomy of the Heart by Multislice Computed Tomography*. Oxford, UK: Wiley-Blackwell, pp. 81–87.
5. Mas MS & Bricker JT. (1990) Clinical physiology of left-to-right shunts. In: Garson A Jr., Bricker JT, McNamara DG (eds). *The Science and Practice of Pediatric Cardiology*. Pennsylvania: Lea & Febiger, pp. 999–1001.
6. Murphy GJ, Gersh BJ, McGoon MD, *et al.* (1990) Long-term outcome after surgical repair of isolated atrial septal defect: follow-up at 27–32 years. *N Engl J Med* **323**:1644–1650.
7. Meissner I, Khandheria BK, Heit JA, *et al.* (2006) Patent foramen ovale: innocent or guilty? Evidence from a prospective population-based study. *J Am Coll Cardiol* **47**:440–445.
8. Webb G & Gatzoulis MA. (2006) Atrial septal defects in the adult: recent progress and overview. *Circulation* **114**:1645–1653.
9. Carminati M, Hausdorf G, Tynan M, *et al.* (1997) Initial clinical experience of transcatheter closure of secundum atrial septal defect with a septal occlusion device. *Eur Heart J* **19**(Suppl.):136.

10. Vida VL, Barnoya J, O'Connell M, *et al*. (2006) Surgical versus percutaneous occlusion of ostium secundum atrial septal defects: results and cost-effective considerations in a low-income country. *J Am Coll Cardiol* **47**:326 –331.
11. Masani ND. (2001) Transoesophageal echocardiography in adult congenital heart disease. *Heart* **86**(Suppl. 2):II30–II40.
12. Magni G, Hijazi Z, Pandian NG, *et al*. (1997) Two- and three-dimensional transesophageal echocardiography in patient selection and assessment of atrial septal defect closure by the new DAS-Angel wings device: initial clinical experience. *Circulation* **96**:1722–1728.
13. De Castro S, Cartoni D, Fiorelli M, *et al*. (2000) Morphological and functional characteristics of patent foramen ovale and their embolic implications. *Stroke* **31**:2407–2413.
14. Acar P, Saliba Z, Bonhoeffer P, *et al*. (2001) Assessment of the geometric profile of the Amplatzer and Cardioseal septal occluders by three dimensional echocardiography. *Heart* **85**(4):451–453.
15. Marx GR, Fulton DR, Pandian NG, *et al*. (1995) Delineation of site, relative size and dynamic geometry of atrial septal defect by real-time three-dimensional echocardiography. *J Am Coll Cardiol* **25**:482–490.
16. Cao Q, Radtke W, Berger F, *et al*. (2000) Transcatheter closure of multiple atrial septal defects. Initial results and value of two- and three-dimensional transoesophageal echocardiography. *Eur Heart J* **21**:941–947.
17. Van Mierop LH & Kutsche LM. (1985) Development of the ventricular septum of the heart. *Heart Vessels* **1**:114–119.
18. Crenshaw BS, Granger CB, Birnbaum Y, *et al*. (2000) Risk factors, angiographic patterns, and outcomes in patients with ventricular septal defect complicating acute myocardial infarction: GUSTO-I trial investigators. *Circulation* **101**:27–32.
19. Edwards BS, Edwards WD, & Edwards JE. (1984) Ventricular septal rupture complicating acute myocardial infarction: identification of simple and complex types in 53 autopsied hearts. *Am J Cardiol* **54**:1201–1205.
20. Menon V, Webb JG, Hillis LD, *et al*. (2000) Outcome and profile of ventricular septal rupture with cardiogenic shock after myocardial infarction: a report from the SHOCK trial registry. *J Am Coll Cardiol* **36**:1110–1116.
21. Minette MS & Sahn DJ. (2006) Ventricular septal defects. *Circulation* **114**:2190–2197.
22. Gersony WM, Hayes CJ, Driscoll DJ, *et al*. (1993) Bacterial endocarditis in patients with aortic stenosis, pulmonary stenosis, or ventricular septal defect. *Circulation* **87**(Suppl. I):I121–I126.
23. Topaz O. (2003) The enigma of optimal treatment for acute ventricular septal rupture. *Am J Cardiol* **92**:419–420.
24. Bialkowski J, Szkutnik M, Kusa J, *et al*. (2007) Transcatheter closure of postinfarction ventricular septal defects using Amplatzer devices. *Rev Esp Cardiol* **60**:548–551.
25. Lun K, Li H, Leung MP, *et al*. (2001) Analysis of indications for surgical closure of subarterial ventricular septal defect without associated aortic cusp prolapse and aortic regurgitation. *Am J Cardiol* **87**:1266–1270.
26. Backer CL, Winters RC, Zales VR, *et al*. (1993) Restrictive ventricular septal defect: how small is too small to close? *Ann Thorac Surg* **56**:1014–1018.
27. Pesonen E, Thilen U, Sandstrom S, *et al*. (2000) Transcatheter closure of post-infarction ventricular septal defect with the Amplatzer septal occluder device. *J Scand Cardiovasc* **34**:446–448.
28. Rigby M & Redington A. (1995) Primary transcatheter umbrella closure of perimembranous ventricular defect. *Br Heart J* **73**:368–371.
29. Acar P, Abdel-Massih T, Douste-Blazy MY, *et al*. (2002) Assessment of muscular ventricular septal defect closure by transcatheter or surgical approach: a three-dimensional echocardiographic study. *Eur J Echocardiogr* **3**:185–191.
30. Kardon RE, Cao QL, Masani N, *et al*. (1998) New insights and observations in three-dimensional echocardiographic visualization of ventricular septal defects. *Circulation* **98**:1307–1314.
31. Chen FL, Hsiung MC, Nanda N, *et al*. (2006) Real time three-dimensional echocardiography in assessing ventricular septal defects: an echocardiographic-surgical correlative study. *Echocardiography* **23**:562–568.
32. De Castro S, Caselli S, Papetti F, *et al*. (2006) Feasibility and clinical impact of live three-dimensional echocardiography in the management of congenital heart disease. *Echocardiography* **23**:553–561.
33. Acar P, Abadir S, & Aggoun Y. (2007) Transcatheter closure of perimembranous ventricular septal defects with Amplatzer occluder assessed by real-time three-dimensional echocardiography. *Eur J Echocardiogr* **8**:110–115.
34. Thanopoulos BD & Rigby ML. (2005) Outcome of transcatheter closure of muscular ventricular septal defects with the Amplatzer ventricular septal defect occluder. *Heart* **91**:513–516.
35. Balzer J, Kühl H, Rassaf T, *et al*. (2008) Real-time transesophageal three-dimensional echocardiography for guidance of percutaneous cardiac interventions: first experience. *Clin Res Cardiol* **97**:565–574.